Chapter-II

ZrO_2/MgAl-LDH composite and evaluation of its isotherm, kinetics and thermodynamic properties in the adsorption of congo red dye

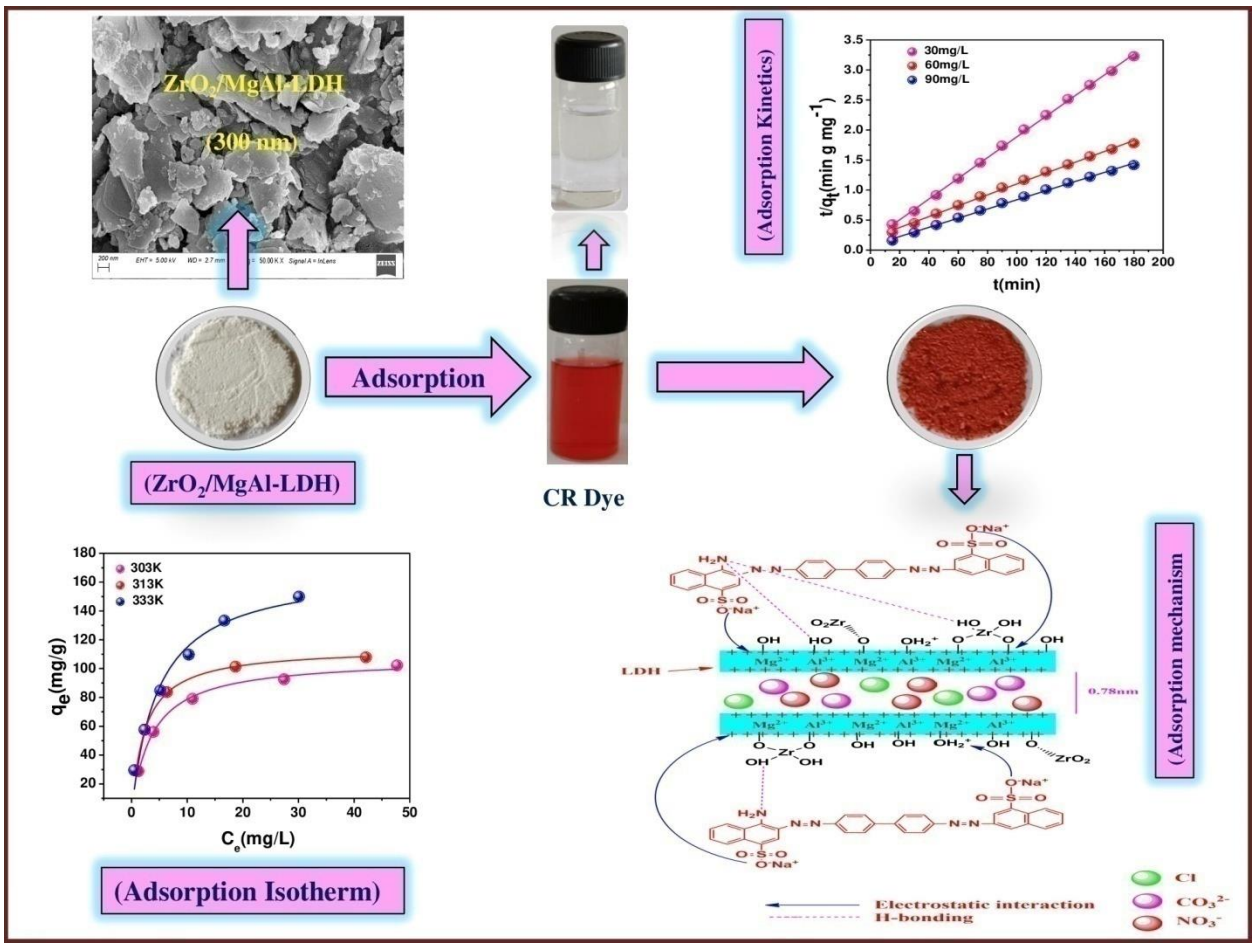

Chapter-II

ZrO_2/MgAl-LDH composite and evaluation of its isotherm, kinetics and thermodynamic properties in the adsorption of congo red dye

II.1 Introduction

With the rapid expansion of modern industries, the increasing emissions of potentially toxic synthetic dyes have caused severe global threat to the environment, affecting aquatic systems and other habitats living in the ecosystem.[1,2] Despite their high toxic effect, synthetic dyes are also widely used in various industries such as textile, paper, paint, food, pharmaceuticals, cosmetics, and plastics for dyeing purposes. Currently, synthetic azo dyes are the major water pollutants that are discharged from several manufacturing industries and carried directly to natural water bodies, including rivers, oceans, canals, lakes, and other geographical region.[3,4] Accounting for its stable chemical structure, non-biodegradable, and toxic nature, azo dye can change the biochemical characteristics of the fresh water system, which in turn leads to adverse effects on aquatic life. In addition, the presence of such organic pollutants can also decrease biological oxygen demand and increase chemical oxygen demand.[5,6-7] Nearly, 7×10^5 tons of varieties of dye are manufactured anually all over the world. In particular, congo red (CR) dye is one of the most extensively used dyes, which decomposes into benzidine compound, and it is known for its potential effect to cause carcinogenic activities in living creatures.[8,9-10] Concerning public health and environmental protection regulation, development of environmental remediation material for the elimination of CR dye from effluent before releasing it into the environment is very crucial and could be an interesting research field.

Over the past two decades, numerous waste water remediation techniques, including photocatalytic degradation, reverse osmosis, membrane filtration, flocculation, magnetic separation, and electrodialysis have been employed. Nevertheless, most of these methods involve high costs, low removal capacity, critical processes, high energy consumption, and the generation of secondary waste products. Consequently, these methods are not appropriate for large scale treatment of dye contaminated waste water.[11,12-16] Alternatively, the adsorption method has proven to be an excellent process for the separation of dye stuff contaminants. Owing to its reversible nature, robust, universal approach, low cost, high efficiency, easy separation, and simple operation, this technique has great potential to be utilized for a large scale

industrial applications in developing nations. Several adsorbent materials for decontamination of waste water are available, which include agricultural waste-derived activated carbon,[17] metal organic frameworks,[18] zeolite,[19] polymer-based gels,[20] grapheme oxide nanomaterials,[21] and clay minerals.[22] Moreover, in search of outstanding adsorption performances and to make sustainable adsorbents, the fabrication of these materials to enhance their adsorption characteristics is gaining considerable attraction among researchers. For instance, Hu et al. have reported a polyacrylic superadsorbent hydrogel, synthesized via free radical polymerization by using nano spherulites (CNS) crosslinkers, which display a large adsorption capacity (2100 mg/g) for methylene dye.[20] Mosavi et al. prepared MOF-5 through the solvothermal method and modified it with $CuCl_2$ at ambient temperature, which is further adapted for CR adsorption.[18] Mao et al. fabricated pristine graphene oxide and synthesized interconnected reduced graphene oxide and fluorinated graphene oxide, and its adsorptive performance in aqueous medium was examined by implementing water pollutant dyes such as rhodamine B and methylene blue, where the maximum adsorption capacity obtained was 686.6 mg/g and 403.3 mg/g, respectively.[21]

Layered double hydroxide (LDH), also known as anionic clays, are the hierarchically structured materials containing brucite sheets composed of divalent M^{2+} and M^{3+} cations with interlayer anions A^{2-} such as OH^-, CO_3^{2-}, and Cl^- etc. The electroneutrality in the structure is ensured by the colombic force of attraction between intergallery anions and positive charge metals on the LDH layer.[23] Due to its wide range of applications, including flame retardant, drug delivery, adsorbents, and catalysis, layered double hydroxide can be regarded as an exceptionally promising material. Consequently, researchers find it interesting to further explore the ability of LDH to evaluate the issues emerging due to azo-dye contaminants. Among the clay materials, LDHs are the most versatile material, which displays excellent dye removal characteristics during the water purification process. The structure of LDH is flexible and possesses important structural features such as porosity, high surface area, anion exchangeability, isomorphic substitution of metal ions on brucite sheets, surface modification, and transformation to mixed metal oxides upon calcinations at 500 °C. Nevertheless, low cost and less toxic nature of LDH are also other advantages making it more viable and environmentally benign material for removal of hazardous organic contaminants from effluents.[24,25]

Based on the literature, most of the LDH employed for wastewater treatment are generally containing monovalent to trivalent cations in their structure. However, modification with tetravalent cations can alter the charge of LDH sheets, which may enhance their sorption characteristics. Since Zr-based sorbents are known for their effective removal of various inorganic and organic contaminants, this can be attributed due to the high positive charge of Zr ions, which possess a strong tendency for electronegative ions. Besides, zirconium has also been manifested as a non-toxic, ecofriendly, and cost effective metal precursor.[26] Thus, the synthesis of the composite material ZrO_2/MgAl-LDH by fabricating LDH with Zr salts may benefit the resulting adsorbent by making it more sustainable and also due to the integration of characteristic features of both LDH and Zr(IV) metal oxide. Additionally, it might widen its sorption properties, which are not only limited to anionic dyes, but the removal of several other harmful inorganic ions such as F^-, PO_4^{2-}, and AsO_2^- could be feasible. On that account, grabbing the advantage of both Zr(IV) metal oxide and LDH, the present work mainly focuses on the development of a novel composite material, viz., ZrO_2/MgAl-LDH, by adopting urea hydrolysis method and evaluating its adsorption efficiency by taking CR dye as a model pollutant. The synthesized adsorbent ZrO_2/MgAl-LDH is well characterized, and the influence of various experimental factors such as adsorbent dosages, contact time, ionic strength, co-existing anions, pH, and temperature is investigated. The adsorption isotherm and kinetics model are used for fitting experimental data. In order to analyze the adsorption mechanism, powder XRD and FT-IR spectra after adsorption are recorded.

II.2 Experimental

II.2.1 Materials and Methods

Zirconium oxychloride ($ZrOCl_2.8H_2O$), Aluminium chloride ($AlCl_3$), and Magnesium chloridehexahydrate ($MgCl_2.6H_2O$) were purchased from Merck. Urea (NH_2CONH_2) and CR ($C_{32}H_{22}N_6Na_2O_6S_2$) (purity = 98%) were obtained from Qualigens India Pvt. Limited. All the chemicals are of analytical grade and are used without any further purification. The required solution for adsorption experiments is prepared by using distilled water.

II.2.1.1 Synthesis of the ZrO_2/MgAl-LDH composite

The synthesis of ZrO_2/MgAl-LDH was prepared by urea hydrolysis method. Initially, a mixture of 3 mmol $MgCl_2.6H_2O$, 1 mmol $ZrOCl_2$, and 2 mmol $AlCl_3$ was dissolved in 100 mL of distilled water taken in a beaker. The resulting solution containing metal precursors was vigorously stirred in a magnetic stirrer. 2.1 g of urea is added further to the solution, followed by continuous stirring for 15 minutes, until the clear homogeneous solution was obtained. This liquid suspension is then transferred into an autoclave and heated in an oven at 150 ℃ for 6 hours. The resulting white precipitate was then centrifuged at 800 rpm and washed with distilled water up to five times. The obtained slurry was dried in an oven at 50 ℃ for 12 hours. Finally, the white product is ground with mortar to get powder form, which is denoted as ZrO_2/MgAl-LDH.

II.2.1.2 Characterization

The synthesized sample ZrO_2/MgAl-LDH was characterized by different spectroscopic techniques in order to get detailed information about its physico-chemical properties. The X-ray diffraction pattern was recorded by the Rigaku Ultima-IV powder X-ray diffractometer using CuK_α radiation. The FT-IR spectrum of the sample was recorded on Shimadzu IR Affinity-1 by using KBr background. The thermal decomposition of the adsorbent was studied in TGA (Mettler Toledo) under a N_2 atmosphere at the heating rate of 20 ℃/min and an operating temperature of 30-1100 ℃. The external microstructure was examined by scanning emission microscopy (Gemini Carl Zeiss Sigma 300). The internal morphology was investigated using transmission emission microscopy (JEOL JEM-2100). The specific surface area, and porosity of the sample was determined at 77 K by using the surface area analyser (Quantachrome Novawin version 11.05) by conducting adsorption and desorption of N_2 gas. The atomic composition and valence state of the constituent elements in the sample was estimated by X-ray photoelectron spectroscopy (XPS) (PHI 5000 Versa Probe II). The residual dye concentration was measured using the UV-Spectrophotometer-3375 (Electronics India). The point of zero charge (PZC) of ZrO_2/MgAl-LDH was determined by the pH drift method. Initially, a series of solution at different pH values (3-9) containing 20 mL each of 0.1M NaCl was prepared, while the pH of

the solution was adjusted by using 0.1M HCl and 0.1M NaOH. Subsequently, 0.3 g of the adsorbent was added to each of the prepared solutions, which were further stirred for 24 hours. After completion of stirring, the final pH of the solution was measured by the digital pH meter MK VI, and the point of zero charge (PZC) value was evaluated from the plot of pH initial vs pH final.

II.2.1.3 Adsorption experiment

The various adsorption experiments are conducted in batch mode. In isotherm studies, an aqueous CR dye solution at varying initial concentration (30 mg/L-180 mg/L) containing 20 mL each was taken in a 150 mL conical flask. Thereafter, 0.02 g of the adsorbent ZrO_2/MgAl-LDH was mixed with a CR dye solution, which was followed by agitation in a water bath shaker for a time period of 4 hours to attain equilibrium. The experiment was carried out at operating temperature of 30 ℃, 40 ℃, and 50 ℃. Furthermore, after reaching equilibrium the adsorbent was separated from the solution by filtration, and the residual dye concentration remaining in the filtrate was calculated spectrophotometrically by the UV-Spectrophotometer (EI-3315), which was set at the maximum wave length of 498 nm. The quantity of the CR adsorbed on ZrO_2/MgAl-LDH was estimated by the equation (2.1).

$$q_e = \frac{(C_0 - C_e)\,V}{W} \qquad (2.1)$$

The percentage of dye removal was calculated by the equation (2.2).

$$\text{Percentage of dye removal} = \frac{(C_0 - C_e) \times 100}{C_0} \qquad (2.2)$$

where, C_0 and C_e indicates initial and the equilibrium concentration of CR dye solution in mg/L. q_e(mg/g) signifies the equilibrium adsorption capacity, V is the total volume of solution in litres (L) and W denotes amount of adsorbent in gram (g).

For kinetic studies, the experiment was performed under a constant temperature of 30 ℃. Initially, 0.02 g of adsorbent was dispersed in 40 mL of CR dye solution at different initial

concentration (30, 60 and 90 mg/L). The resulting solution is then agitated in a thermostatic shaker similar to the isotherm experiment for a time period of 180 minutes. However, 2 mL of the solution is withdrawn after a definite time interval, which is separated from the adsorbent by centrifugation at 1000 rpm/min. After separation, the concentration of residual dye is analyzed to determine the rate of dye adsorption with time. The CR dye uptake by the adsorbent with time was evaluated by the equation (2.3).

$$q_t = \frac{(C_0 - C_t)\,V}{W} \qquad (2.3)$$

where, q_t (mg/g) is the amount of dye uptake at time t(min), V is the total volume of the solution(L), W is the quantity of adsorbent (g), and C_0 and C_t are the concentration of dye at initial and at time t, respectively.

II.2.1.4 Desorption Studies:

The desorption experiment was investigated by using eluents of different natures, such as acetone, ethanol, methanol, 0.1 M NaOH, and 0.1 M Na_2CO_3. Initially, 20 mL of CR dye solution at a 40 mg/L concentration was allowed to be treated with 0.015 g of ZrO_2/MgAl-LDH for a contact time of 3 hours. After complete adsorption, the adsorbent was separated from the suspension and dried. Subsequently, the dye-loaded adsorbent was further agitated in a 20 mL eluent solution to desorbed the initially adsorbed dye molecule under the same reaction time. The percentage of desorption was calculated by the equation (2.4).

$$\text{Desorption \%} = \frac{C_{desorbed}}{C_{sorbed}} \times 100 \qquad (2.4)$$

where, $C_{desorbed}$ and C_{sorbed} are the quantity of dye desorbed and adsorbed, respectively.

II.2.1.5 Error Analysis

To test the best fitting of isotherm data with different adsorption isotherm model, χ^2 value was computed which is represented by the following equation (2.5).[27]

$$\chi^2 = \sum \frac{(q_{e,exp} - q_{e,cal})^2}{q_{e,exp}} \qquad (2.5)$$

where $q_{e,exp}$ is the equilibrium sorption capacity calculated from experiment and $q_{e,cal}$ is the equilibrium sorption capacity predicted by the isotherm model.

However, for determining the most appropriate kinetic model that can describe the sorption process, the sum of the squares error was evaluated by the equation (2.6).[28]

$$\text{Sum of square error } (SSE) = \frac{\sqrt{\sum(q_{e,cal} - q_{e,exp})^2}}{N} \qquad (2.6)$$

where, $q_{e,cal}$ is the equilibrium sorption capacity evaluated from pseudo-first order and pseudo-second-order kinetic model, $q_{e,exp}$ is the experimental amount of adsorbate adsorbed at equilibrium, N is the number of data points.

II.2.2 Adsorption Isotherm (Langmuir isotherm)

To investigate the affinity of CR dye towards the adsorbent ZrO_2/MgAl-LDH, an adsorption isotherm experiment was conducted. From the isotherm studies, the qualitative nature of the adsorbate-adsorbent system can be well understood. The experimental equilibrium data were fitted based on the four different isotherm models, especially Langmuir, Freundlich, Temkin, and Redlich-Peterson isotherms. According to the Langmuir model, it is assumed that the heat of adsorption is equal for all the adsorption site of the material and the solute molecules are homogeneously adsorbed throughout the surface of the adsorbent.[29]

The non-linear equation for Langmuir model is formulated as:

$$q_e = \frac{q_{max} C_e K_l}{1 + K_l C_e} \qquad (2.7)$$

where, q_{max} and q_e indicate the maximum monolayer adsorption capacity and the amount of dye adsorbed at equilibrium, respectively. K_l signifies the Langmuir constant, which is related to the free energy of adsorption, and C_e (mg/L) denotes the concentration of dye at equilibrium.

In order to interpret the feasibility of the adsorption process, the dimensionless separation factor R_L was computed by the equation (2.8).[30]

$$R_L = \frac{1}{1+K_l C_o} \quad (2.8)$$

where, K_l and C_o(mg/L) are Langmuir constant and initial concentration of dye, respectively.

II.2.2.1 Freundlich Isotherm

The Freundlich isotherm is an empirical equation that describes adsorption in a heterogeneous system and relates the amount of adsorbate intake per unit mass of the adsorbent. The model is generally more appropriate for adsorption on heterogeneous surfaces. The non-linear Freundlich isotherm equation is given as:[31]

$$q_e = K_f\, C_e^{\,1/n} \quad (2.9)$$

where, n and K_f are Freundlich constants related to intensity and adsorption capacity in the sorption process.

II.2.2.2 Temkin Isotherm

Accounting for the interaction with adsorbate-adsorbent system, the Temkin model considers that a linear reduction in the heat of adsorption arises for the solute molecules by increasing the coverage of the sites. The non-linear Temkin isotherm is formulated as:[32]

$$q_e = B_T \ln (K_T C_e) \quad (2.10)$$

where, B_T and K_T indicate the Temkin constant, which implies heat of adsorption (KJ/mol) and equilibrium binding constant (L/mg).

II.2.2.3 Redlich-Peterson Isotherm

The Redlich-Peterson isotherm is a three-parameter isotherm model that includes the elements present in both the Langmuir and Freundlich equations for better fitting with experimental data. Unlike ideal monolayer adsorption, the mechanism of adsorption is unique and shows a combined characteristic mechanism. The nonlinear equation of Redlich-Peterson is given as:[33]

$$q_e = \frac{A\,C_e}{1+BC_e^{\beta}} \qquad (2.11)$$

It is a hybrid model which describes both homogeneous and heterogeneous adsorption by combining both the Langmuir and Freundlich equations. Several studies shows that Redlich-Peterson model is more accurate compare to both models. *A* and *B* are Redlich-Peterson constants, and β is the exponential factor lying between 0 and 1. If β =1, then the Redlich-Peterson equation reduces to Langmuir whereas for β =0 it is transformed to Freundlich equation.

II.2.2.4 Adsorption Kinetics

To further analyze the rate of dye adsorption and the mechanism involved, kinetics studies were executed and further examined by using the five most widely used models, such as pseudo-first-order, pseudo-second-order, intraparticle diffusion, Bangham, and Boyd. Based on the pseudo first order kinetic model, it is assumed that the adsorption process is physical in nature and that the rate of solute intake is proportional to the ratio of the concentration of the solute to the quantity of adsorbent. The pseudo-first-order equation is represented as:[34]

$$\log (q_e - q_t) = \log q_e - \frac{K_1\,t}{2.303} \qquad (2.12)$$

where q_e and q_t signify the amount of dye adsorbed at equilibrium and at time t, respectively. K_1 is the first order rate constant, which is obtained from the slope of the linear plot log $(q_e - q_t)$ vs *t*. In contrast, the pseudo second order model postulates that the adsorption process involves chemisorption, where there is an interchange of electrons between the solute molecules and the adsorbent used. The pseudo second order kinetic equation is given as:[35]

$$\frac{t}{q_t} = \frac{1}{K_2 q_e^2} + \frac{t}{q_e} \qquad (2.13)$$

where, q_t, q_e, t has their usual meaning and K_2 is the second order rate constant, which is evaluated from the intercept of the linear plot of t/q_t vs *t*. Besides, the intraparticle diffusion

model proposed by Weber-Morris assumes that there is a possibility for the diffusion of solute molecules into the pores present on the surface of the adsorbents, which may affect the rate-limiting step during the adsorption process. The equation for the intraparticle diffusion model is presented as:[36]

$$q_t = K_i t^{0.5} + C \quad (2.14)$$

where, K_i and C are the intraparticle diffusion constant and boundary layer thickness, respectively, which are determined from the slope and intercept of the linear plot q_t vs $t^{0.5}$.

To further elucidate the actual process that controls the overall rate of sorption, a complex mathematical expression proposed by Boyd was applied to the kinetics data. This model helps in distinguishing between boundary layer diffusion and pore diffusion. The Boyd equation is formulated as:[37]

$$F = (1- \frac{6}{\pi^2}) \exp(-B_t) \quad (2.15)$$

$$B_t = - 0.4977 - \ln(1-F) \quad (2.16)$$

$$F = \frac{q_t}{q_e} \quad (2.17)$$

$$B = \frac{\pi D_i}{r^2} \quad (2.18)$$

where q_t(mg/g), q_e(mg/g) are the quantity of dye adsorbed at time t and at equilibrium, B_t is the mathematical function of F, D_i is the diffusion coefficient and r denotes radius of the adsorbent particle (m). The value of B was determined from the slope of B_t vs t plot.

In general, the rate limiting step during the sorption process in several adsorbate-adsorbent systems could be only due to pore diffusion. As a result, to confirm the possibility of pore diffusion in the ZrO_2/MgAl-LDH-CR system, it is further interpreted by fitting the kinetics data based on the Bangham equation. The Bangham equation is represented by the given equation:

$$\log [\log (\frac{C_o}{C_o - mq_t})] = \log (\frac{K_o m}{2.303V}) + \alpha \log t \quad (2.19)$$

where, K_o and α are Bangham constant, C_o indicates initial dye concentration (mg/L), q_t represents amount of dye adsorbed at any time *t*, *V* is the volume of solution (mL) and *m* denotes the weight of the adsorbent (g).

II.3 Results and Discussions

II.3.1 Characterization of ZrO_2/MgAl-LDH

The powder X-ray diffraction (P-XRD) spectrum of ZrO_2/MgAl-LDH is presented in **Fig II.1**. The diffraction pattern reveals sharp and intense peaks which are corresponding to indexed plane 003, 006, 009, 015, 018, 110, 113. The observed characteristic peaks are consistent with a typical LDH diffraction pattern reported in previous work.[39] The diffractograms of the synthesized sample reveal the formation of pure sample ZrO_2/MgAl-LDH. Moreover, the highly intense and sharp peaks occur at lower 2θ values, while with an increasing 2θ value at a higher angle, the intensity of peak decreases. The absence of broad peaks infers a crystalline phase in the sample. The lattice parameters a and c of ZrO_2/MgAl-LDH was evaluated theoretically by the expression $a=2d_{110}$ and $c=3d_{003}$. The parameter a represents an intermetallic distance in LDH, and c is related to the thickness of the interlayer, which relies on the positively charged density of LDH sheets and intergallery anions. The calculated values are summarized in **Table II.1** It is obvious from the obtained results that the calculated cell parameters a=3 Å and c=23.4 Å of ZrO_2/MgAl-LDH is found almost similar to the MgAl-LDH synthesized in the previous literature. However, the incorporation of Zr ions having a large ionic radius in brucite sheets should increase intermetallic distance a, whereas in our study it is seen that lattice parameter a value does not increase, which reveals that Zr ions are not introduced inside LDH sheets rather it exists as ZrO_2 phase. In addition, **Fig II.1** does not reveal the diffraction pattern of crystalline ZrO_2, which can be due to its existence as an amorphous phase. Nevertheless, it can be suggested that sample is a composite material containing MgAl-LDH and an amorphous ZrO_2 phase.[40] After adsorption of CR dye molecules, a new peak arises at diffraction angle 2θ of 32.40, 35.57, 42.81, 53.72, and 50.37, which can be ascribed to surface adsorbed CR molecules. Besides, there are no significant changes observed in cell parameters a and c before and after adsorption. From **Fig II.1** the shifting of peaks corresponding to 003 and 110 was not noticed in ZrO_2/MgAl-CR. The basal spacing d_{003} value was almost identical for both ZrO_2/MgAl-LDH (0.78 nm) and (CR) adsorbed

ZrO_2/MgAl-LDH-CR (0.77 nm). Consequently, it can be envisaged that the adsorption of CR dye takes place on external surfaces via weak interactions such as H-bonding, electrostatic forces and surface complexation rather than intercalation between the interlamellar regions.[41]

TableII.1: The characteristics cell parameters of ZrO_2/MgAl-LDH before and after the adsorption of CR dye.

Adsorbent	d_{003} (Å)	d_{009} (Å)	d_{110} (Å)	a (Å)	c (Å)
ZrO_2/MgAl-LDH	7.8	2.60	1.5	3	23.4
ZrO_2/MgAl-LDH-CR	7.7	2.61	1.5	3	23.1

d = d-spacing, Å = Angstrom, CR = Congo red dye, LDH = Layered double hydroxide, Cell parameters = a, c

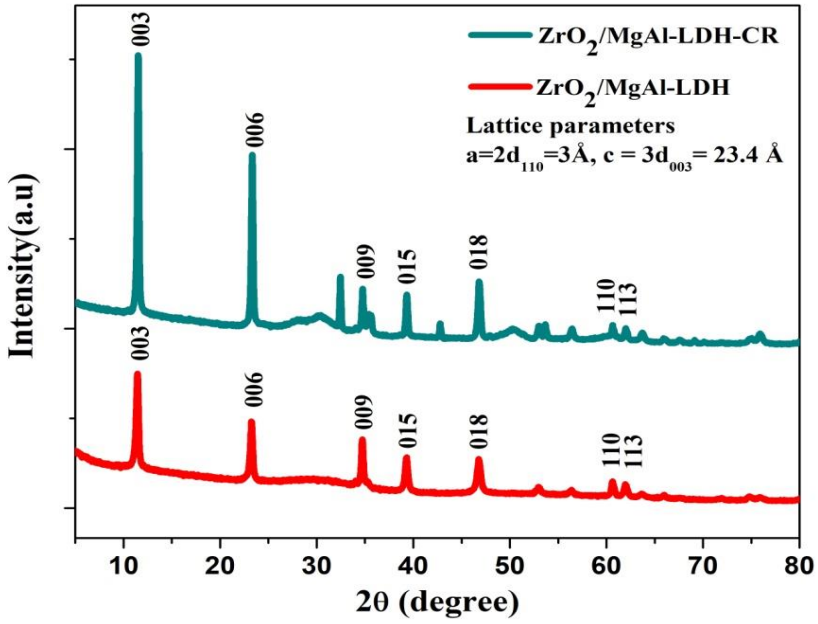

Fig II.1: XRD pattern of ZrO_2/MgAl-LDH and CR adsorbed ZrO_2/ MgAl-LDH-CR.

The FT-IR spectroscopy technique has been used to analyze the stretching vibration of existing functional groups present on adsorbents. **Fig II.2(a-c)** demonstrates the FT-IR spectrum of ZrO_2/MgAl-LDH, congo red dye, and ZrO_2/MgAl-CR after adsorption of CR dye molecules. In pristine ZrO_2/MgAl-LDH **(Fig II.2a)**, the broad band at 3457 cm^{-1} arises due to the stretching

vibration of υ-OH functional group present on metal hydroxide brucite layers. Another band observed at 1628 cm^{-1} may be attributed to the –OH bending vibration of interlayer water molecule. A weak band at 1354 cm^{-1} may be due to the presence of asymmetric stretching vibrations of CO_3^{2-} ions. Since LDH has a strong affinity for CO_2, a small amount of atmospheric CO_2 gets adsorbed. The broad absorption band at 781 cm^{-1} can be assigned to Mg-Al-O vibration, and the less intense weak band at 685 cm^{-1} can be accounted for by M-O stretching vibrations. Moreover, after adsorption of the CR dye molecule in **Fig II.2c**, the appearance of a new small peak at 1231 cm^{-1} could be due to the S=O stretching vibration of the dye adsorbed on the LDH surfaces. The obtained result confirms the successful intake of CR dye over the proposed adsorbent ZrO_2/MgAl-LDH.[42,43]

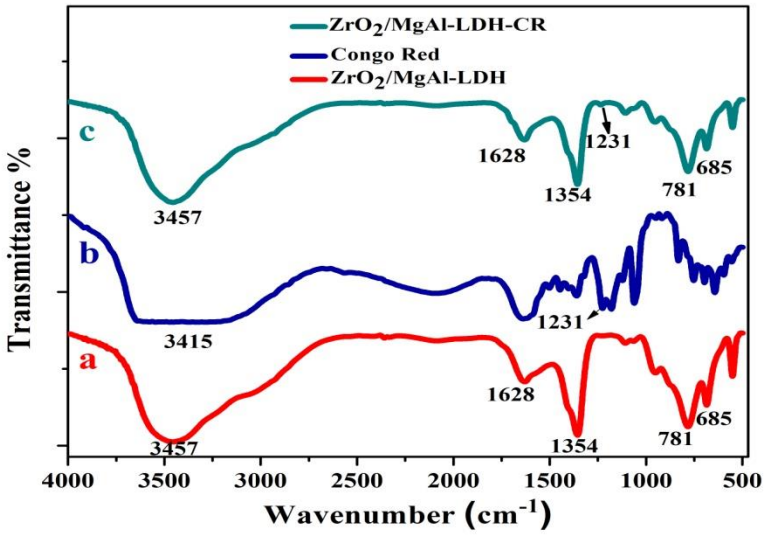

Fig II.2: FT-IR spectra (a) ZrO_2/MgAl-LDH (b) Congo red (c) ZrO_2/MgAl-LDH -CR

In general, the adsorption property of the adsorbent is greatly influenced by its specific surface area and porosity, which can provide imperative information about sorption characteristics. Consequently, it is essential to measure structural properties such as surface area and porosity, which are conducted by the BET adsorption method. The N_2-adsorption-desorption isotherm and pore size distribution of ZrO_2/MgAl-LDH are presented in **Fig II.3(a).** The estimated BET specific surface area, pore volume, and pore diameter are 71.55 m^2/g, 0.119 cc/g,

and 3.04 nm, respectively. The inset of **Fig II.3(a)** indicates that the pore size distribution lies in the range between 3.22 nm to 8.15 nm. However, it is seen that the area of the pore size distribution is narrow, which reveals that the distribution of pores is uniform throughout the structure. The sample ZrO_2/MgAl-LDH exhibits type IV isotherm with an H-4 hysteresis loop, which infers the mesoporous nature of the materials based on the IUPAC classification.[44]

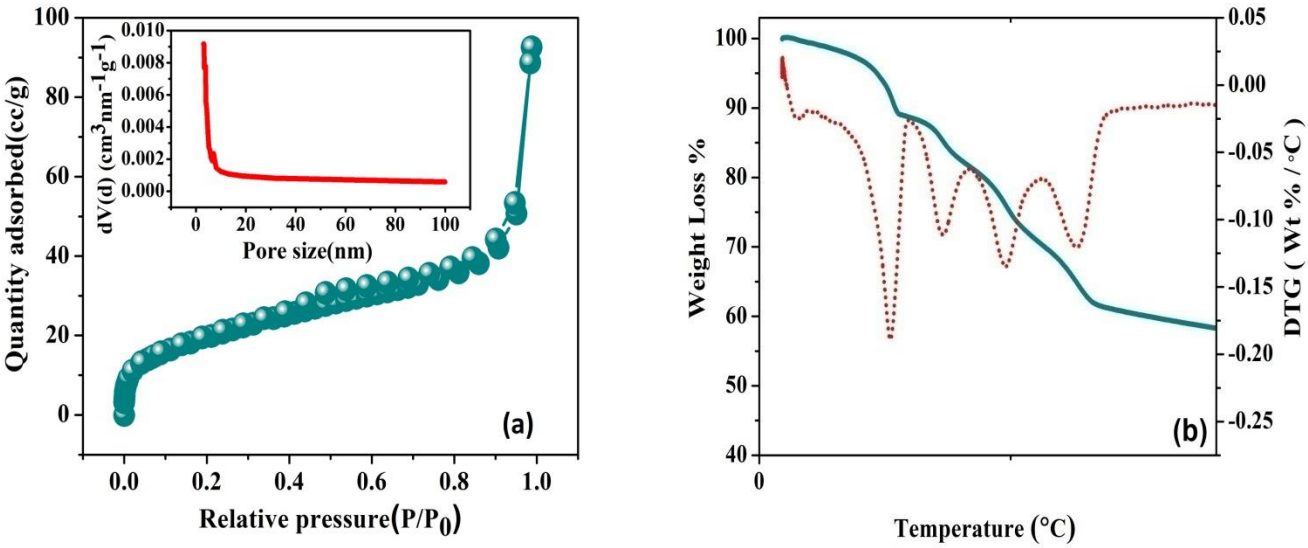

Fig II.3: (a) N_2 adsorption-desorption isotherm and pore sized distribution of ZrO_2/MgAl-LDH (b) Thermogravimetric analysis of ZrO_2/MgAl-LDH.

The thermal stability of ZrO_2/MgAl-LDH was investigated by TGA, which is depicted in **Fig II.3b**. The TGA profile reveals that weight loss takes place in four steps, as noted by exothermic peaks in DTG curves. The initial weight loss of 11.26 % in the first step lying below 262 ℃ may be attributed to the evaporation of physically adsorbed water molecules. In the second and third step, the small amounts of weight loss 5.83 % and 8.95 % identified between 263-446 ℃ were observed due to the removal of interlayer ions such as Cl^-, CO_3^{2-}, and OH^-. The mass loss of 12.97 % in the last stage indicates the complete breakdown of LDH structure into mixed metal oxide due to the complete dehydroxylation of brucite layers. After 610 ℃ there is no further weight loss observed, leading to a constant straight-line curve.[45,46]

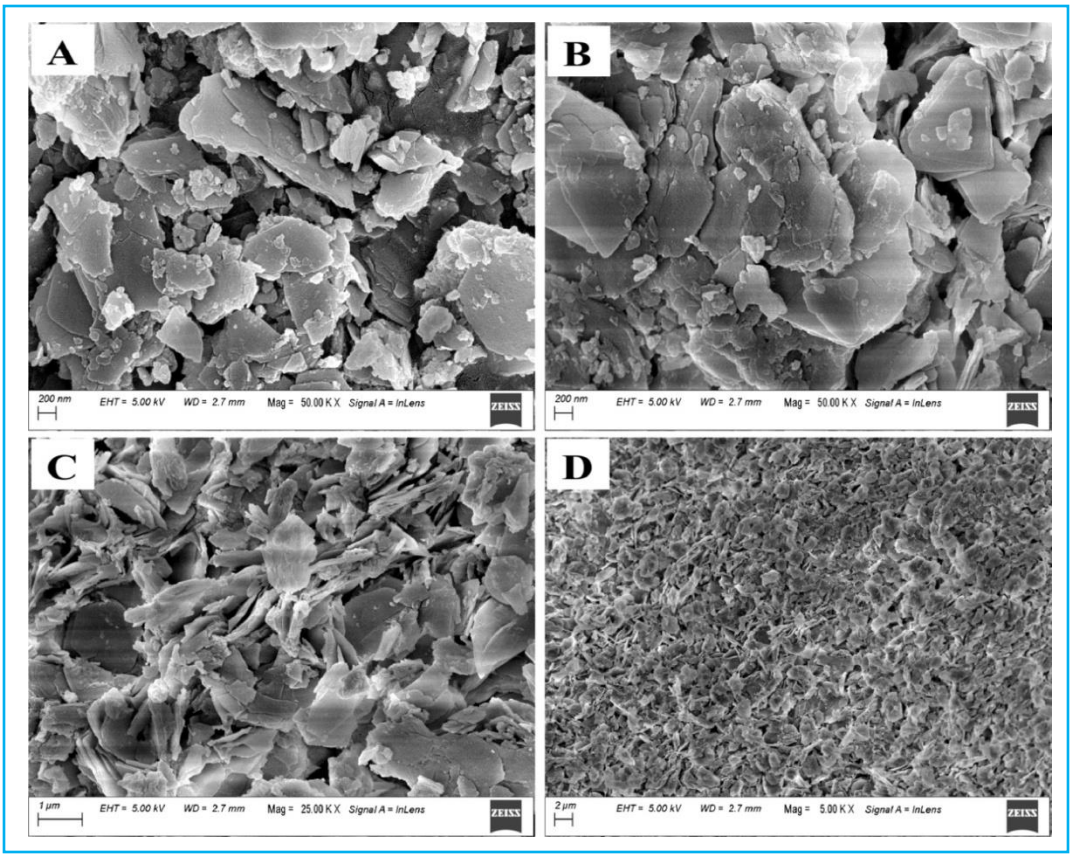

Fig I.4: FE-SEM micrograph (A-D) of ZrO_2/MgAl-LDH at different resolution (200 nm, 1µm and 2 µm)

FE-SEM images of ZrO_2/MgAl-LDH depict the detailed surface morphology at different resolution, which is shown in **Fig II.4(A-D)**. The image confirms the aggregation of plate-like particles at a resolution below 1 µm, which is typical for LDH morphology. The hexagonal-shape LDH platelets are found stacked upon one another at an average size greater than 1µm. From the analysis of the FE-SEM micrograph, it is also evident that the surface feature of LDH is not uniform and reveals the existence of pores between LDH platelets.[47] **Fig II.5** reveals the elemental composition of the ZrO_2/MgAl-LDH composite obtained by energy dispersive x-ray (EDX) analysis. It is obvious that the main constituent elements present in the adsorbents in terms of weight percentage are Zr(13.92 %), Mg(19.38 %), Al(11.50 %) and O(55.20 %), respectively.

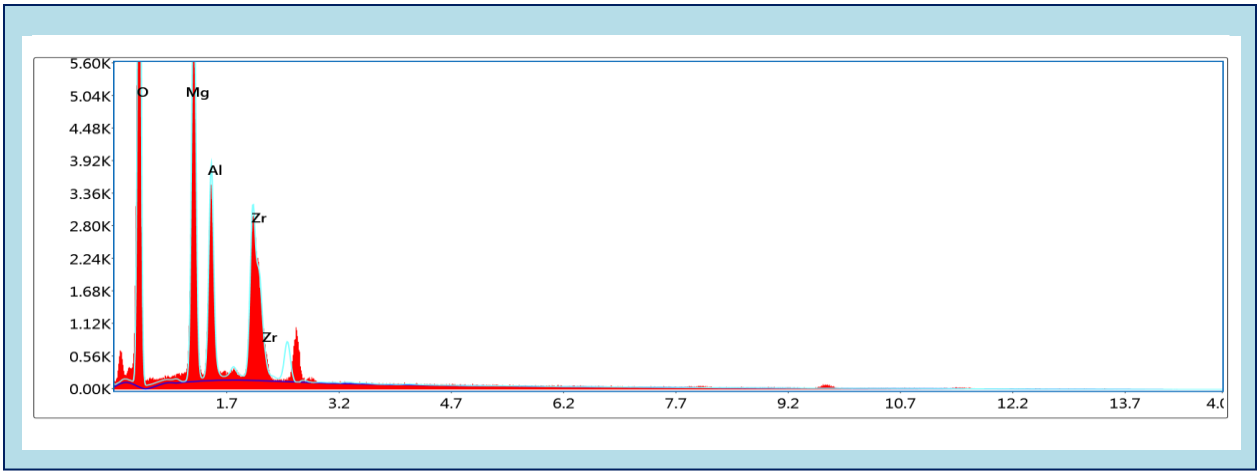

Fig II.5: EDX spectra of ZrO_2/MgAl-LDH composite.

The high-resolution TEM micrograph of ZrO_2/MgAl-LDH is presented in **Fig II.6(A-F)**. It is seen that in **Fig II.6(A)**, the evaluated lattice fringes d_{009} (0.26 nm) corresponding to the 009 plane of ZrO_2/MgAl-LDH was manifested, which is consistent with powder XRD results. **Fig II.6(C-E)** depicts the structure of LDH platelets. The pattern observed in the selected area electron diffraction shown in **Fig II.6(F)** conforms to the polycrystalline nature of the materials. In addition, the d-spacing values of 0.26 nm, 0.2 nm, and 0.14 nm was measured from the SAED pattern, which can be related corresponding to 009, 018, and 110 planes.[48]

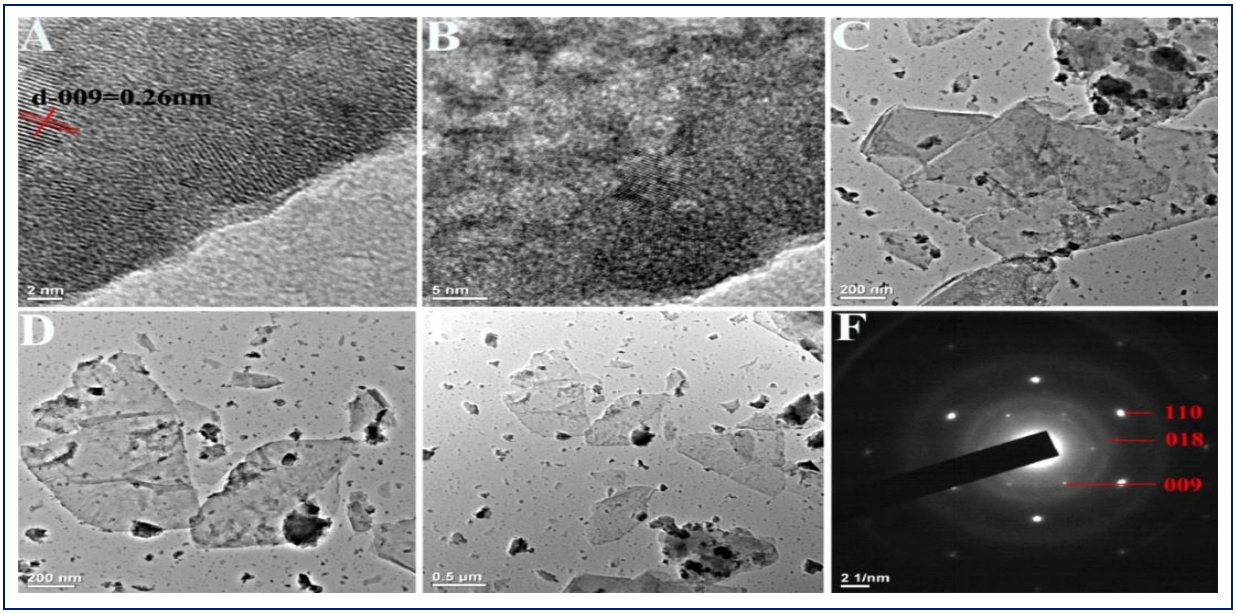

Fig II.6: HRTEM images (A-E) and SAED pattern (F) of ZrO_2/MgAl-LDH composite.

Fig II.7(a) depicts the full XPS spectrum of ZrO_2/MgAl-LDH, which shows the presence of constituting elements such as Zr, Mg, Al, O, and C. The XPS spectra of C 1s presented in **Fig II.7(b)** reveal three peaks at 291.82 eV, 293.57 eV, and 295.76 eV, which can be accounted for due to the small quantity of atmospheric CO_2 adsorbed on LDH. The peak for O 1s was visible at 539.09 eV, which may be ascribed to the CO_3^{2-} and OH^- ion present in the LDH structure.[49] In **Fig II.7(f)**, the doublet peak corresponds to Zr-O-Zr bonds, while Zr (3d) has a binding energy of 186.94 eV and 191.16 eV with energy separation (4.22 eV), which are mainly contributed from Zr $3d_{5/2}$ and Zr $3d_{3/2}$, respectively. Besides, the peak noted at a binding energy of 337 eV corresponds to Zr $3p_{3/2}$, as shown in **Fig II.6(a)**. The existence of Zr metal in $3p_{3/2}$ and $3d_{5/2}$ states affirms its oxidizing nature. Additionally, the Zr metal in ZrO_2 form having a +4 valency state in the composite material can also be anticipated. In general, the binding energy of Zr for the valency state (0, +1, +2, +3) lies in the range (178 to 184 eV) as per the results reported by Lackner et al. The peak corresponding to Mg 2s and Al 2p was obtained at 75.49 eV and 96 eV, respectively.[50,51]

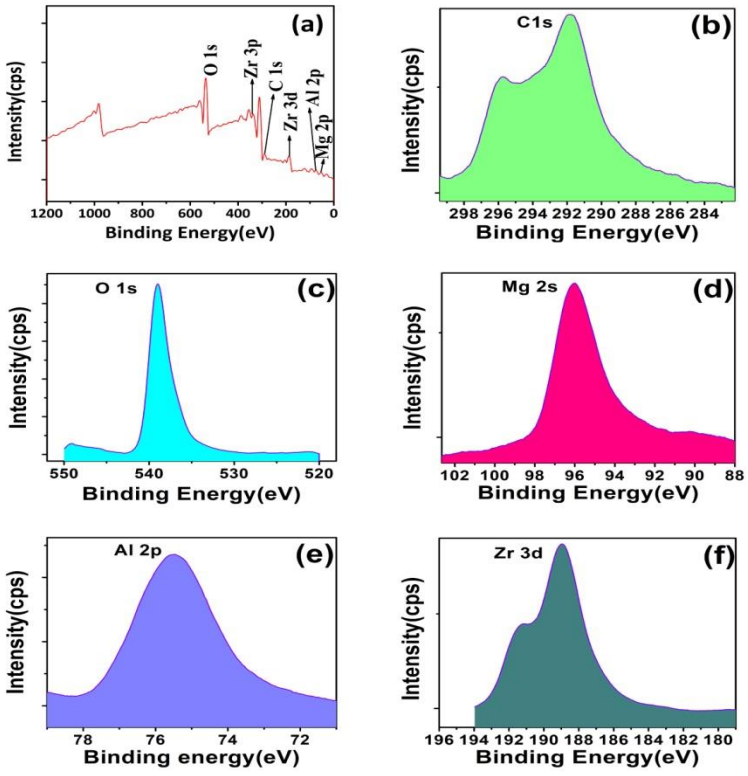

Fig II.7: XPS spectra of ZrO_2/MgAl-LDH (a- wide scan, b- C1s, c- O1s, d- Mg2s, e- Al 2p, f- Zr3d).

II.3.1.1 Effect of adsorption parameters

II.3.1.2 Effect of pH

During the adsorption process, the pH of the solution plays a significant role, which can have an impact on the structure and charge of the sorbents. It can influence the dissociation of functional group presents on the binding sites of adsorbents; besides, it also affects the solubility of solutes in aqueous solutions. **Fig II.8(a)** demonstrates the removal efficiency of CR by ZrO_2/MgAl-LDH over a pH ranging between 4-9. The pH of the dye solution is varied from 4-9, while other parameters in the reaction conditions, such as adsorbent dosages, temperature, contact time, initial dye concentration, and volume of solution were fixed at 0.02 g, room temperature, 90 minutes, 50 mg/L and 20 mL, respectively. According to the observed results shown in **Fig II. 8(a)**, it implies that the effects of pH change are remarkable and possess characteristic information regarding the interaction between adsorbate and adsorbent molecules. The maximum removal of CR dye (81.96 %) was achieved at pH 4, while on increasing pH from 4 to 9, there is a continuous decrease in the dye removal percentages, which declines up to 58.64 %. In general, below pH 4, the structure of LDH breaks down and loses its adsorption property. However, the characteristic variation displayed in the removal efficiency of ZrO_2/MgAl-LDH can be well understood from the ionic chemistry of the solution and the charge of the sorbents.[24,52] Consequently, the point of zero charge (PZC) described in terms of pH value, where the net charge on the adsorbent surface is zero, was estimated by pH drift method.

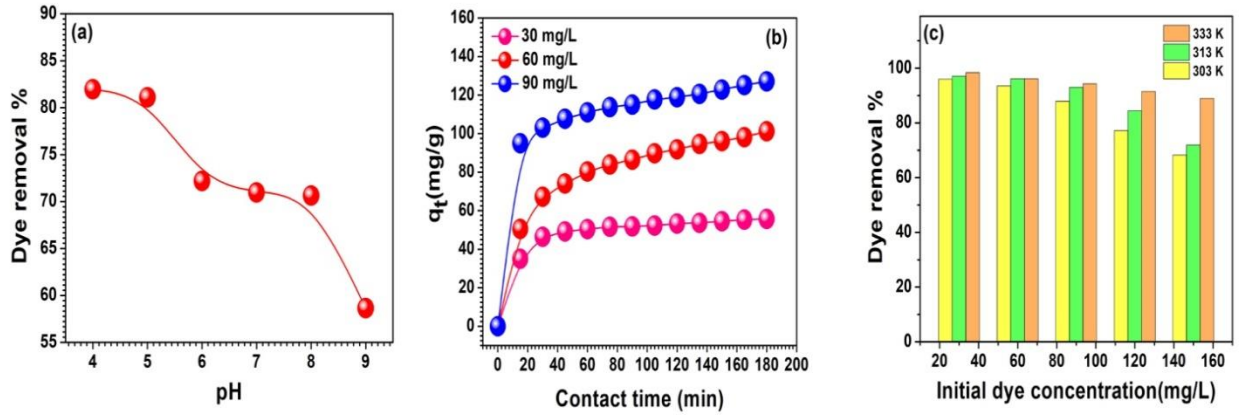

Fig II.8: Effect of various parameters for adsorption of CR dye over ZrO_2/MgAl-LDH (a) pH (C_0=50 mg/L, adsorbent dosages=0.02 g, time=90 min, volume=20 mL). (b) Contact time (C_0= 30, 60, 90 mg/L, adsorbent dosages=0.02 g, time=90 min, volume=40 mL) (c) Initial dye concentration (C_0=30-150 mg/L, adsorbent dosages=0.02 g, time=240 min, volume=20 mL, temperature= 303-333 K).

Fig.II.8: (d) (d) Adsorbent dosages (C_0=50 mg/L, time= 240 min, volume=20 mL).

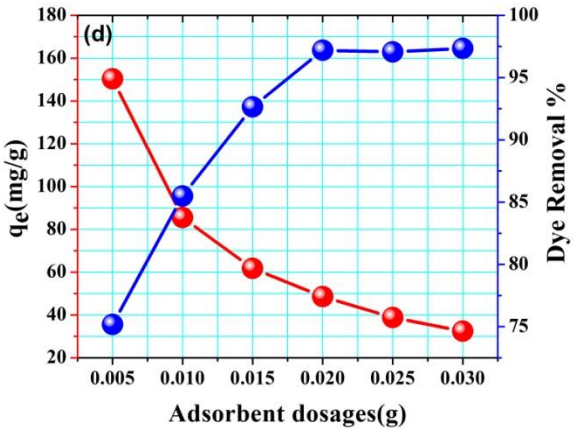

From **Fig II.9**, the point of intersection in the pH initial vs pH final plot lies at 5.49, which refers to the point of zero charge value (PZC). At pH values less than PZC, around 4 to 5.49, the presence of a greater number of protonated ions H^+, which accumulate on the LDH surfaces, provides additional positive charges on the ZrO_2/MgAl-LDH. These positive charges on the ZrO_2/MgAl-LDH surface attracts the negatively charge anionic dyes more strongly and are bound with the help of electrostatic forces. In contrast, at pH>PZC (5.49), the surface of the particle becomes negatively charged, and the existing hydroxyl ion competes with the incoming negative charged anionic dyes for the adsorption sites. Hence, the adsorption capacities of ZrO2/MgAl-LDH get reduced with increasing pH. Nevertheless, the main factor on which adsorption of CR over ZrO_2/MgAl-LDH strongly depends on the electrostatic forces between functional groups of dyes and positive charge LDH sheets.[34,53]

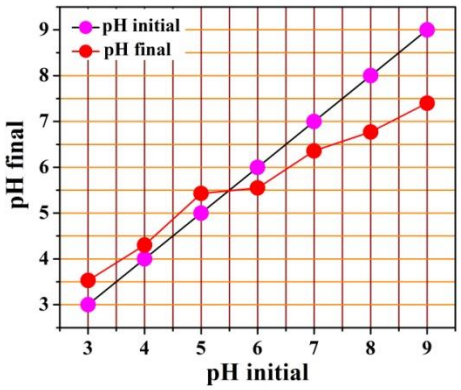

Fig II.9: Determination of the point of zero charge (PZC) value of ZrO_2/MgAl-LDH from pH initial vs pH final plot.

II.3.1.3 Effect of contact time

The contact time between adsorbate and adsorbent is another important parameter to be investigated during the sorption process. The effect of contact time on the adsorption of CR dye by ZrO_2/MgAl-LDH at different initial dye concentrations (30, 60, 90 mg/L) is depicted in **Fig II. 8(b)**. The result obtained manifests that at the initial stage of contact time up to 20 minutes, the rate of dye adsorption is fast for all the concentration of CR dye. It can be attributed to the large number of adsorption site and the high concentration gradient of dye at the initial stage, which can promote the rapid intake of solute dye molecules.[22,54] Subsequently, the inflexion of the curve observed in the region between 20 and 50 minutes can be ascribed to the slow diffusion of dye molecules inside the pores of LDH; therefore, the rate of adsorption becomes slow. However, the equilibrium state of CR adsorption was achieved near the contact time of 180 minutes. In addition, with the progress of adsorption process, access to the remaining vacant site is less available for sorption because of the steric repulsion between the incoming solute molecules and the adsorbed molecules.[55] After complete saturation at 180 minutes, the maximum q_t value obtained corresponding to initial concentrations of 30 mg/L, 60 mg/L, and 90 mg/L are 55.74, 101.19 and 127.14 mg/g, respectively.

II.3.1.4 Effect of initial dye concentration

The effect of initial dye concentration on adsorption over ZrO_2/MgAl-LDH was investigated by varying the concentration from 30-150 mg/L under the reaction temperature of 303 K, 313 K, and 333 K, as shown in **Fig II.8(c)**. The results clearly indicate that there is a gradual decrease in dye removal percentage with an increase in the initial concentration of solute at all temperatures. This can be attributed to the limited number of active sites in the adsorbent due to the increasing solute concentration. In general, at a low initial dye concentration, the adsorption process is mainly monolayer, which is further extended to multilayer until the equilibrium stage is reached at high solute concentrations. Moreover, the driving force required is more to overcome the mass transfer resistance of solute molecules between solid and liquid phase at high dye concentrations.[43,56] The dye removal efficiency decreases from 95.90-68.18%, 97-71.91%, and 98.33-88.87% at 303 K, 313 K, and 323 K, respectively. In addition, dye removal efficiency is found to be higher at 323 K.

II.3.1.5 Effect of dosages

To account for the cost-effectiveness of the system, it is important to evaluate the optimum dosages of adsorbent. The influence of dosages on the removal efficiency of CR dye was examined by changing the quantity of adsorbent from 0.005 g to 0.030 g, which is presented in **Fig II.8(d)**. It is obvious that the percentage removal of dye increases initially with an increase in adsorbent amount until 0.02 g, beyond these dosages, the removal percentage remains almost similar. This can be attributed to the presence of a greater number of available adsorption sites with increasing adsorbent dosages. However, it was noted that there were no remarkable changes observed in adsorption performances after 0.02 g. Moreover, excessive use of adsorbents beyond optimum ranges can lead to the aggregation of LDH particle due to collision, which can restrict the accessible adsorption site for the incoming dye molecules by decreasing the specific surface area and increasing the diffusion path length value.[43,57] On the other hand, it is observed that the equilibrium adsorption capacity q_e decreases from 150.34 mg/L to 32.44 mg/L with increasing dosages of 0.005 g to 0.030 g. Moreover, the maximum removal efficiency up to 97.19% was achieved at 0.02 g dosages, which can be considered an optimum dosage for the reaction condition fixed at 50 mg/L initial dye concentration and a contact time of 4 hours.

II.3.1.6 Effect of ionic strength and coexisting ions

The effluent discharges from various textile industries have adequate amounts of salts, which can affect the adsorption performances. Consequently, it is important to investigate the effect of ionic strength during the adsorption process. The increasing ionic strength of the solution can either enhance or retard the adsorption of organic dyes, or it may not be effective in some adsorbate-adsorbent systems, which are clearly not known due to less reports. However, the ionic strength is controlled by the nature of the salt, dyes, and adsorbent used during the reaction.[58] In this work the ionic strength is adjusted by adding 0.5 mL each of Na_2CO_3 solution at different strengths from 0.1 M to 0.4 M to the congo red dye solution fixed at initial concentration 50 mg/L and adsorbent dosages of 0.02 g. From the result shown in **Fig II.10(a)**, it was obvious that the removal efficiency of CR dye decreases with an increase in the ionic strength of Na_2CO_3, which may be due to the competition existing between CO_3^- ion and CR dye ions for surface adsorption on ZrO_2/MgAl-LDH. It is noticed that the dye removal % gets reduced from 73.03% to 60.11%.

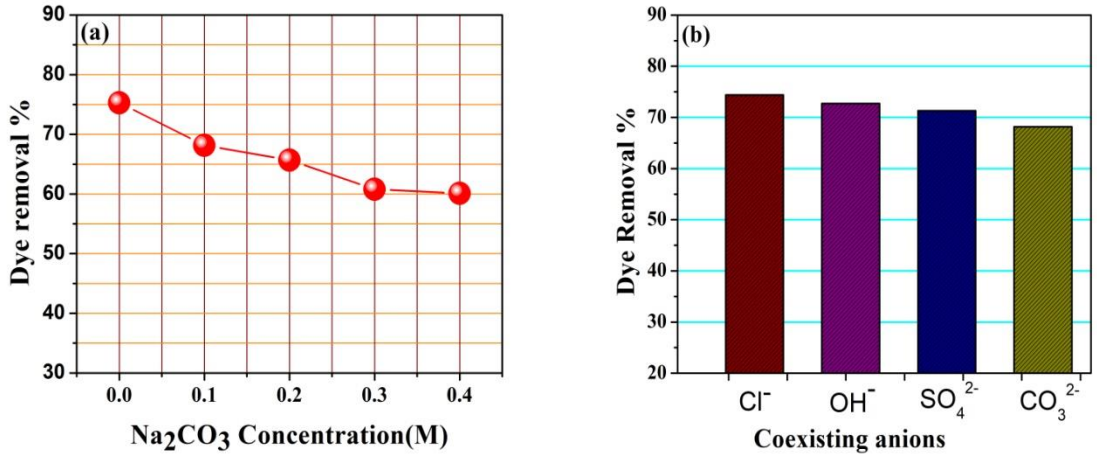

Fig II.10: (a) Effect of ionic strength (C_0 = 50 mg/L, adsorbent dosages = 0.02 g, time = 120 min, volume = 20 mL) (b) Influence of coexisting ions (C_0 = 50 mg/L, adsorbent dosages = 0.02 g, time = 120 min, volume = 20 mL).

The influence of coexisting ions such as OH^-, Cl^-, SO_4^{2-}, CO_3^{2-} on the removal efficiency of congo red dye was examined under the operating conditions: 50 mg/L congo red solution, 0.02 g adsorbent, contact time = 2 hours, 0.5 mL from each of the 0.1 M salt solutions (NaOH, NaCl, Na_2SO_4, Na_2CO_3) was added. The observed result in **Fig II.10(b)** indicates that the competitive effects of coexisting ions are in the order: CO_3^{2-} > SO_4^{2-}> OH^-> Cl^-. Moreover, the dye removal % increases from 68 % to 74.38 %, where the lowest efficiency is found in the case of CO_3^{2-} ions which infers that CO_3^{2-} is more competitive compared to other anions. Nevertheless, it is believed that the divalent ions have more competitive effects than monovalent anions, since the ionic potentials of divalent ions are greater than monovalent ions.[59,60]

II.3.1.7 Effect of agitation speed:

Graphical representation of CR adsorption over ZrO_2/MgAl-LDH as a function of agitation speed is shown in **Fig II.11**. The influence in CR adsorption was conducted by varying the agitation speed from 60 rpm to 240 rpm at a contact time of 60 minutes with 0.015 g adsorbent dosages. The degree of agitation can influence the distribution of solute in bulk solution as well as the creation of boundary film. Usually, the increase in agitation speed can lead to a better interaction between adsorbate and adsorbent molecules by exposing all the vacant sites more effectively to the incoming CR molecules. As a result, the adsorption efficiency was found to

increase from 28.97 to 52.73% by increasing agitation speed. At low agitation speed the contact between the adsorbent and solute molecules was found less which could be responsible for the low sorption percentage. Thus, it also suggests that rate of dye removal is also depended on agitation speed and is relatively faster at greater speed.[61]

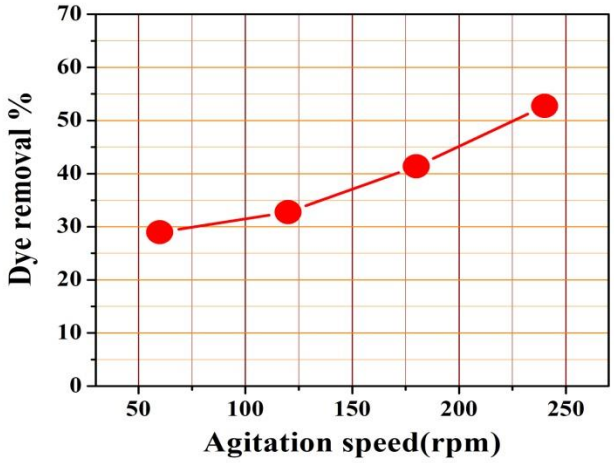

Fig II.11: Effect of agitation speed on the adsorption of CR dye (C_0 = 40 mg/L, dosages = 0.015 g, contact time = 1 hour).

II.3.2 Isotherm Studies

Adsorption isotherm studies can provide qualitative information concerning the adsorption capacity of the adsorbent and the distribution of solute molecules between solid-liquid phases at equilibrium. The isotherm data obtained at 303 K, 313 K, and 333 K were fitted based on the Langmuir, Freundlich, Temkin, and Redlich-Peterson model, which are shown in **Fig II.12(a-d)**. The isotherm parameters of all models are summarized in **Table II.2**. It is evident that after non-linear fitting of the experimental data, the greater coefficient of determination R^2 value is in the order: Redlich-Peterson> Langmuir> Temkin> Freundlich. However, the acceptability of the isotherm model that best fits the experimental data is determined based on the lowest value of χ^2 and closest value of the coefficient of determination (R^2) to unity. Comparing the χ^2 and R^2 value shown in **Table II.2.**, it implies that the two-isotherm model, especially Redlich-Peterson and Langmuir can better explain the studied adsorption process compare to other models. In addition,

it also suggests that the surface of the adsorbent is a combination of both homogeneous and heterogeneous nature.[52,62] **Fig II.13(a)** represents the plot of R_L vs C_o , it is believed that for R_L values lying between 0 and 1, the adsorption process is feasible, while for R_L >1, it indicates an unfavorable process. For irreversible process, R_L is equal to zero. **Table II.2** clearly shows that values of the Langmuir constant lie between 0 and 1, which further indicates that the sorption process is highly favored. Moreover, it is obvious that Freundlich constant n values are greater than 1 at all temperatures, which also implies that the adsorbate molecules are suitably adsorbed on ZrO_2/MgAl-LDH under the operated experimental conditions. The maximum monolayer adsorption capacity of ZrO_2/MgAl-LDH for CR dye at 303 K, 313 K, and 333 K are 107.05, 114.48, and 169.42 mg/g, respectively.

Table II.2: Adsorption isotherm parameters for the adsorption of CR dye onto ZrO_2/MgAl-LDH, obtained from the non-linear fitting of Langmuir, Freundlich, Temkin, and Redlich-Peterson model.

Isotherm model	**Parameters**	**Temperature**		
		303 K	313 K	333 K
Langmuir	q_{max}(mg/g)	107.05 ± 2.28	114.48 ± 1.34	169.42 ± 11
	K_l (L/mg)	0.27 ± 0.02	0.41 ± 0.01	0.21 ± 0.04
	R^2	0.993	0.998	0.970
	χ^2	5.520	2.102	62.249
Freundlich	K_f(mg/g)(L/mg)$^{1/n}$	36.06 ± 5.29	44.85 ± 7.90	44.91 ± 3.63
	n	3.55 ± 0.58	3.93 ± 0.92	2.72 ± 0.21
	R^2	0.927	0.851	0.980
	χ^2	63.42	157.34	40.37
Temkin	B_T	20 ± 1.06	20.66 ± 2.41	30.42 ± 2.57
	K_T	3.88 ± 0.79	6.17 ± 2.84	3.93 ± 1.12
	R^2	0.988	0.947	0.965
	χ^2	9.93	55.762	73
Redlich-Peterson	A (L/g)	36.42 ± 3.60	44.90 ± 3.10	99.31 ± 47.23
	B (L/g)$^{\beta}$	0.43 ± 0.08	0.36 ± 0.05	1.47 ± 0.99
	β	0.932 ± 0.02	1.02 ± 0.02	0.742 ± 0.05
	R^2	0.997	0.998	0.990
	χ^2	1.779	2.117	20.95

Initial Concentration (C_0) = 30-180 mg/L, dosages = 0.02 g, temperature = 303 K, 313 K, 333 K, time = 4 hours, volume = 20 mL

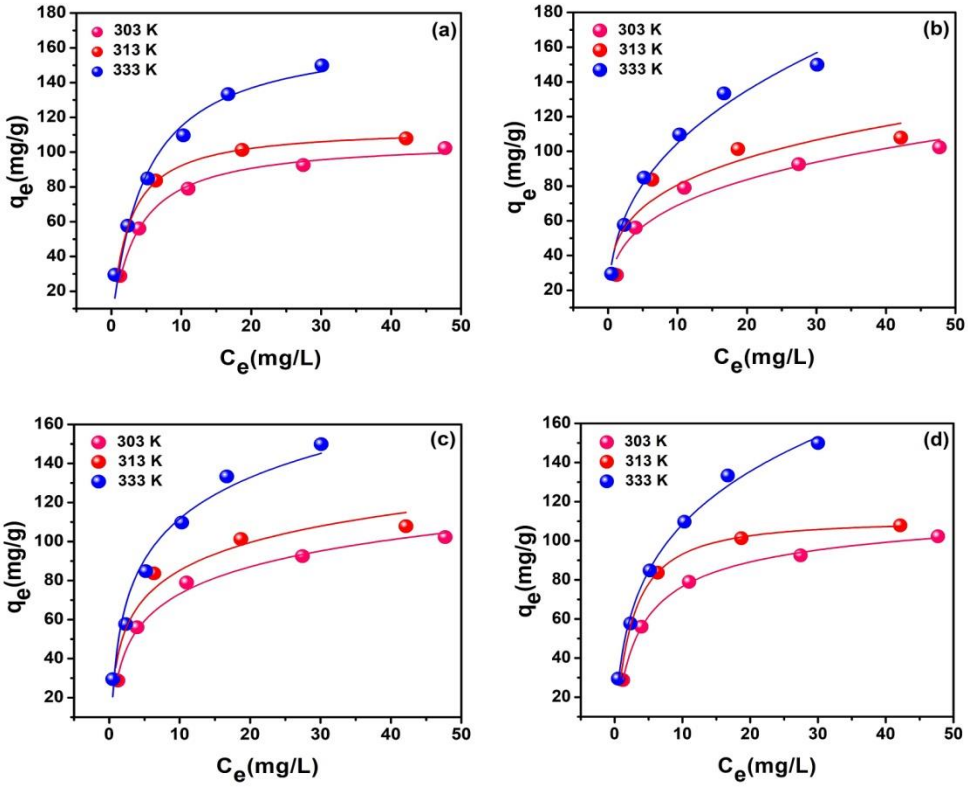

Fig II.12: Non-Linear fitting of various adsorption isotherm model (a) Langmuir (b) Freundlich (c) Temkin (d) Redlich-Peterson for adsorption of CR over ZrO_2/MgAl-LDH.

II.3.3 Kinetics studies

The kinetic parameters of pseudo-first-order, pseudo-second-order, intraparticle diffusion, Boyd, and Bangham model for the adsorption of CR dye by ZrO_2/MgAl-LDH, at different initial concentrations (30, 60, 90 mg/L) is shown in **Table II.3**. The linear fitting of employed kinetic models are demonstrated in **Fig II.13(b-d)**. The suitability of kinetic model was determined by comparing sum of square error (*SSE)* function and of R^2 value. The lower values of SSE and higher values of R^2 are expected to give better fitting in a kinetic model as shown in **Table II.3.** Concomitantly, for all initial dye concentrations (30-90 mg/L), it implies that the obtained kinetics data fit well, according to pseudo-second-order model which can be considered as a predominant mechanism.[30,63] Moreover, the pseudo-second-order rate constant (K_2) constant value decreases with the increase in dye concentration and is in the magnitude of 10^{-4}, the lower values further indicate the longer time taken to attain equilibrium. Besides, the q_{e2} value which

is calculated by the pseudo-second-order model resembles the experimental $q_e$value more closely compare to pseudo first order which further envisages that the associated rate controlling mechanism during the adsorption process can be best described by the pseudo-second-kinetic model. The second order rate constant K_2 corresponding to initial concentrations 30 mg/L, 60 mg/L and 90 mg/L is (18.55, 4.18, 1.82) $\times 10^{-4}$ g.mg^{-1}min^{-1}, respectively.

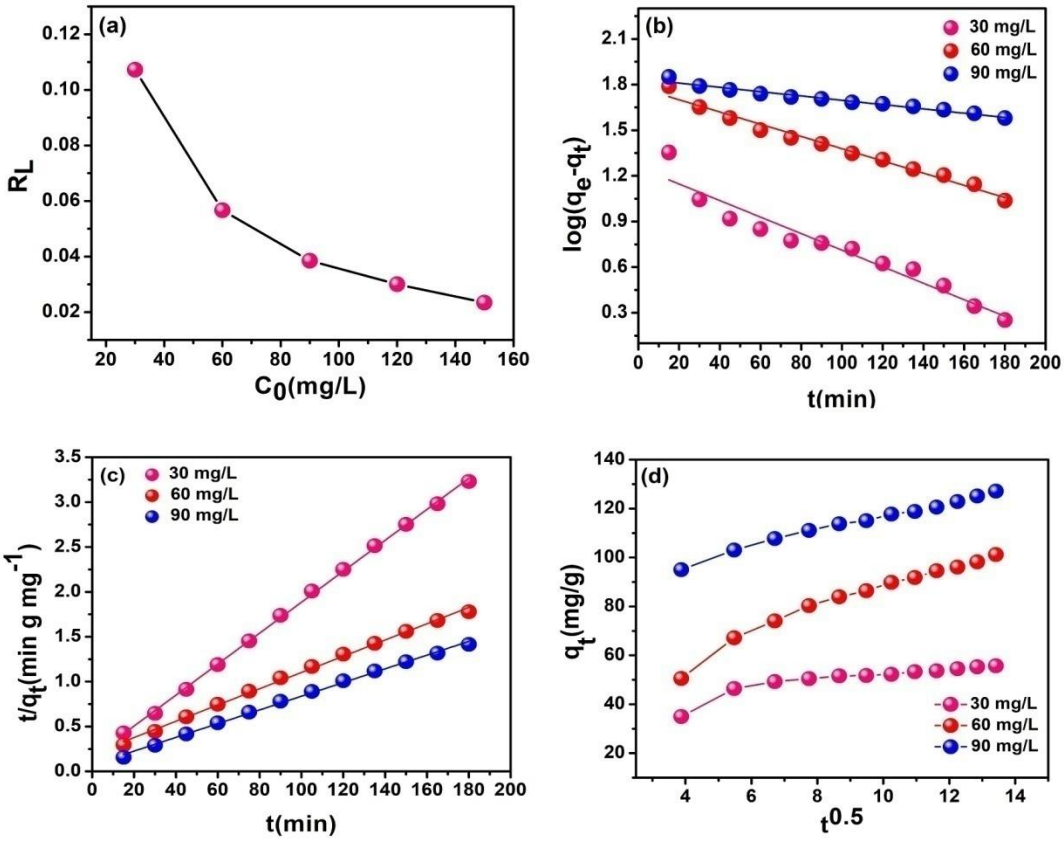

Fig II.13: (a) R_L vs C_0 plot at 303 K (b) Pseudo-first-order kinetics plot (c) Pseudo-second-order kinetics plot (d) Intraparticle diffusion plot.

Furthermore, the plot of q_t vs $t^{0.5}$ displayed in **Fig II.13(d)** clearly reveals the existence of multiple steps during the adsorption process. The initial step represents adsorption on the freely available external adsorption site, while in the middle region, it indicates diffusion of dye molecules inside the pores, and the last step represents the equilibrium stage where complete adsorption on vacant sites was achieved. According to this model, if the linear plot passes through the origin, then intraparticle diffusion controls the rate of adsorption kinetics. But from **II.13(d)** it is clearly seen that the plot did not pass through the origin, which manifests that

although the adsorption process involves intraparticle diffusion, it is not the sole rate-limiting step. In addition, the thickness of boundary layer *C* increases (35.15–85.63 mg/g) with the increase in CR dye concentration (30-90 mg/L), which can be explained on the basis of the increasing boundary layer effect due to the instantaneous occupation of readily available adsorption sites.[52,64]

Table II.3: Parameters of pseudo-first-order, pseudo-second-order and intraparticle diffusion model for the adsorptive removal of CR by ZrO_2/MgAl-LDH.

Kinetics model	**Parameters**	**Initial concentration**		
		30 mg/L	60 mg/L	90 mg/L
Pseudo-first-order	q_e*(exp)*	57.53	112.12	166
	q_{e1}(mg/g*)*	17.98	60.39	68.94
	$K_1 \times 10^{-2}$ min^{-1}	1.25	0.92	0.32
	R^2	0.931	0.979	0.967
	SSE	3.29	4.30	8.08
Pseudo-second-order	q_{e2}(mg/g)	57.97	110.37	130.89
	$K_2 \times 10^{-4}$ ($g.mg^{-1}min^{-1}$)	18.55	4.18	1.82
	R^2	0.999	0.997	0.997
	SSE	0.036	0.145	2.925
Intraparticle diffusion	K_i($mg/g.min^{-1}$)	1.654	4.735	3.092
	C(mg/g)	35.15	39.81	85.63
	R^2	0.768	0.949	0.983
Boyd	$D_i \times 10^{-15}$ (m^2/min*)*	0.319	0.236	0.083
	B	0.012	0.009	0.003
	R^2	0.931	0.980	0.967
Bangham	K_0	34.44	17.93	31.38
	α	0.156	0.261	0.113
	R^2	0.925	0.988	0.997

Initial Conc. (C_0 = 30, 60, 90 mg/L), dosages = 0.02 g, volume = 40 mL, time = 180 min, temp = 30 °C

The dual nature of the adsorbent particle, especially film and pore diffusion during the sorption process, can be easily identified by analyzing the Boyd plot. The graph of B_t vs t at different initial dye concentration (30, 60, 90 mg/L) is illustrated in **Fig II.14(a).** The plot was found to be almost linear for all concentrations and did not pass through the origin; thus, film diffusion seems to be governing the sorption rate of CR dye onto the ZrO_2/MgAl-LDH composite, but it is not the only rate-controlling step. The values of the effective diffusion coefficient D_i (cm^2/min) were evaluated according to equation (2.18) and summarized in **Table II.3.** In this study, the D_i value was found to increased with the increase in concentration of CR dye, which can be attributed to the greater concentration gradient at high CR content.[65]

The graph of log [logC_0/C_0-$q_t m$)] vs log t based on the Bangham equation is presented in **Fig II.14(b)**. The values of the parameters K_0 and α were evaluated from the intercept and slope of the graph, as shown in **Table II.3**. The experimental data modeled by the equation (2.19) corresponding to the initial dye concentration (60, 90 mg/L) showed a linear plot, while for lower concentration (30 mg/L), it did not yield desired linear fit. The higher coefficient of determination (R^2) value obtained from this model also suggests a good fit with the experimental data. This observation further conveys the applicability of this model, which can perfectly explain adsorption kinetics data as pore diffusion-controlled adsorption. Thus, from the overall results obtained in kinetic studies, it can be concluded that both film and pore diffusion play a key role at different stages of the sorption process.[38]

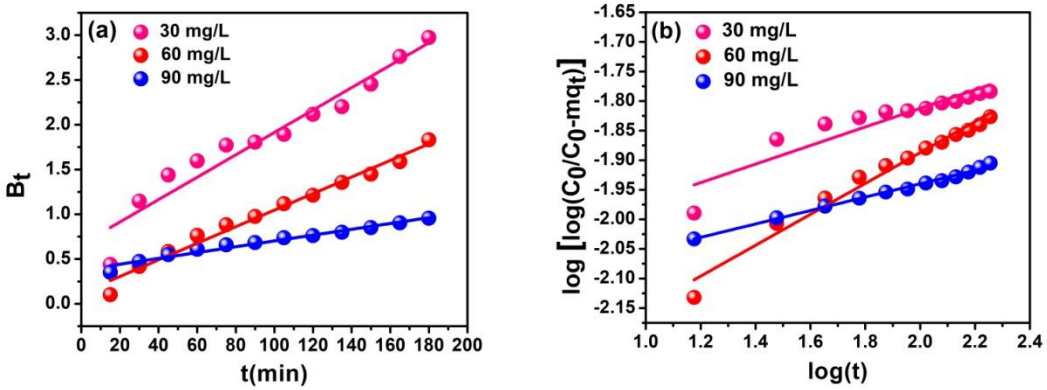

Fig II.14: (a) Boyd kinetic plot and (b) Bangham kinetic plot.

II.3.4 Thermodynamic studies

Temperature is an essential parameter that can affect the adsorption process by influencing the mobility and solubility of the adsorbate and also by changing the equilibrium adsorption capacity. The thermodynamic studies of the adsorption process were executed by subjecting them to various reaction temperatures (303 K, 313 K, 333 K) corresponding to the initial dye concentration (30 mg/L, 120 mg/L), whereas other parameters in reaction conditions, usually adsorbent dosages and contact time, are fixed at 0.02 g, 4 hours, respectively. The essential thermodynamic parameters, such as ΔG, ΔH, and ΔS were evaluated. For thermodynamic studies, the equation for the determination of related parameters is formulated as:[55,66]

$$\Delta G = -RT \ln K_d \qquad (2.20)$$

$$\ln K_d = \frac{\Delta S}{R} - \frac{\Delta H}{RT} \qquad (2.21)$$

where, $K_d\,(C_e\,/q_e)$ signifies adsorption distribution coefficient, ΔG indicates standard free energy (KJ/mol), R denotes universal gas constant, T is the temperature in Kelvin, ΔH is the standard enthalpy (KJ/mol), and ΔS represents standard entropy (J/mol).

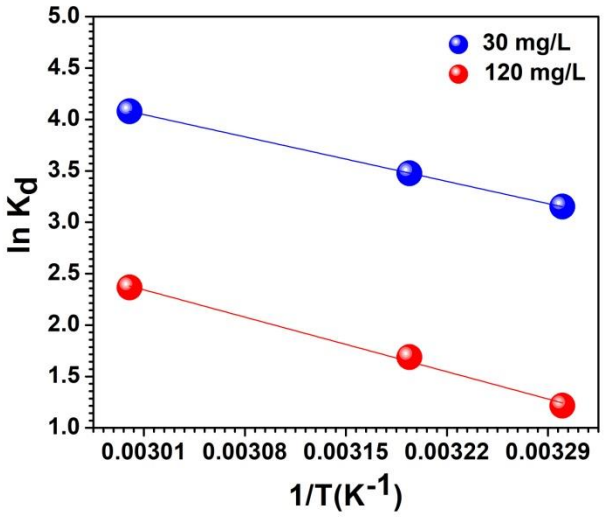

Fig II.15: Vant-Hoff plot for the adsorption behavior of the CR by the adsorbent ZrO_2/MgAl-LDH. (C_0 = 30,120 mg/L, temperature = 303 K, 313 K, 333 K, adsorbent dosages = 0.02 g, volume = 20 mL, contact time = 240 min).

The Vant-Hoff plot shown in **Fig II.15** is obtained from the linear plot of ln K_d versus 1/T. The standard entropy ΔS and enthalpy ΔH can be determined from the intercept and slope of the plot. The thermodynamic parameters are demonstrated in **Table II.4**. It was noted that for both initial dye concentration (30,120 mg/L) with the increasing temperature from 303 K to 333 K the negative value of ΔG is observed, which infers that the adsorption of CR dye by ZrO_2/MgAl-LDH is spontaneous in nature. The standard free energy ΔG decreases from -7.94 to -11.29 KJ/mol and -3.06 to -6.54 KJ/mol for initial dye concentration 30 mg/L and 120 mg/L, respectively. Nevertheless, the obtained ΔH values are positive (+25.70 KJ/mol, +31.51 KJ/mol), which refers to endothermic nature during the adsorption process. The positive ΔS value also signifies the increase in randomness of adsorbate molecules on solid liquid phase. Furthermore, it has been found that the adsorption of CR increases at higher temperature, which indicates more feasibility at 333 K.

To further discern whether the adsorption process is governed by chemisorption or physisorption, the activation energy (E_a) and sticking probability (S^*) value during the thermodynamic studies was estimated from the modified Arrhenius equation which is expressed by the following equation:[67]

$$S^* = (1- \theta)\, e^{-Ea/RT} \qquad (2.22)$$

$$\theta = \left(1- \frac{C_e}{C_o}\right) \qquad (2.23)$$

$$\ln S^* = \ln (1- \theta) - \frac{E_a}{RT} \qquad (2.24)$$

$$\ln (1-\theta) = \ln S^* + \frac{E_a}{RT} \qquad (2.25)$$

where, C_0 and C_e are the initial and equilibrium concentration of dye solution (mg/L), θ denotes surface coverage, E_a (KJ/mol) signifies activation energy, T is the temperature in Kelvin, S^* indicates sticking probability which is dependent on the adsorbate- adsorbent system.

Table II.4: Thermodynamic parameters for the CR uptake on to ZrO_2/MgAl-LDH.

C_0	T(K)	K_d	ΔG(KJ/mol)	ΔH(KJ/mol)	ΔS(J/mol.K)	E_a (KJ/mol)	S^*
30 mg/L	303	23.39	-7.94	25.708	111.032	25.15	0.1913×10^{-5}
	313	32.33	-9.04				
	333	59.11	-11.29				
120 mg/L	303	3.37	-3.062	31.513	114.332	27.04	0.4943×10^{-5}
	313	5.41	-4.395				
	333	10.65	-6.549				

Initial Conc. (C_0) = 30, 120 mg/L, dosages = 0.02 g, time = 4 h, temperature = 303 K, 313 K, 333 K

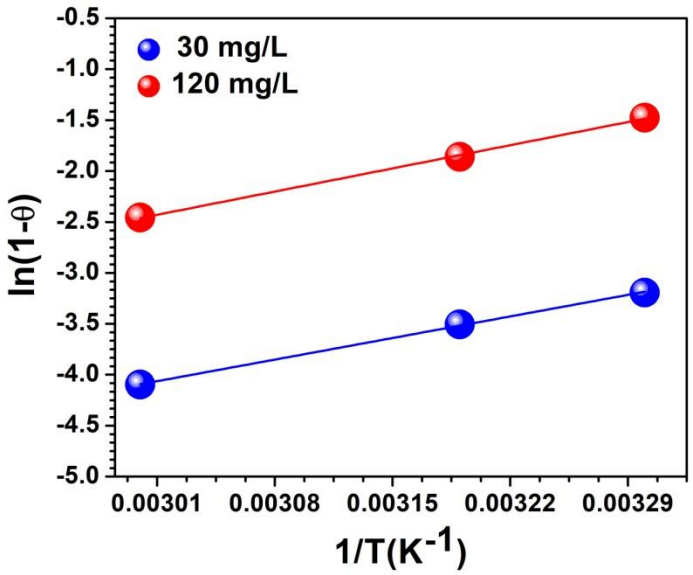

Fig II.16: Modified Arrhenius plot for the adsorption behavior of the CR by the adsorbent ZrO_2/MgAl-LDH. (C_0 = 30,120 mg/L, temperature = 303 K, 313 K, 333 K, adsorbent dosages = 0.02 g, volume = 20 mL, contact time = 240 min).

The plot of ln(1-θ) versus 1/T was depicted in **Fig II.16**, and the values of the thermodynamic parameters E_a and S^* are presented in **Table II.4**. It is evident that the activation energy (E_a)

values obtained corresponding to the initial CR dye concentration 30 mg/L and 120 mg/L are 25.15 KJ/mol and 27.04 KJ/mol, respectively. The sticking probability was found between ($0<S^{*}<1$). Usually, the chemisorption mechanism has activation energy (E_a) ranging between (40-800 KJ/mol), while in the case of physisorption, a relatively lower E_a (5-40 KJ/mol) is associated with the process. Since the activation energy of CR adsorption lies between 5 and 40 KJ/mol, this further implies the existences of a low potential energy barrier. Thus, it can be suggested that the adsorption of CR dye over the ZrO_2/MgAl-LDH composite involved physisorption as a dominant process.[68]

II.3.5 Mechanism of Congo red adsorption on ZrO_2/MgAl-LDH

The plausible adsorption mechanism of CR dye onto ZrO_2/MgAl-LDH composite is depicted in **Fig II.17.** To further analyze the adsorption mechanism, FT-IR and powder XRD spectra are recorded after the adsorption experiment, which are presented in **Fig II.1 and Fig II.2**, respectively. As it is confirmed from the powder XRD spectra of ZrO_2/MgAl-CR displayed in **Fig II.1**, it does not reveal any significant changes in the peak position corresponding to 003 and 110 planes, which further suggests that insertion of adsorbate molecules between interlayer space of LDH sheets does not occur; rather, it is held on the adsorbent surfaces through a combination of several weak and strong bond interactions. Since the adsorption mechanism is dependent on the solution pH, it occurs differently at varying pHs. At lower pH values, the –OH group of the LDH surface gets partially protonated, thereby making it relatively suitable for the strong interaction with the $-SO_3^-$ anion. In contrast, at higher pH values, the repulsion between OH^- and SO_3^- counteracted the electrostatic interaction, where only anion exchangeability may be possible for adsorption. Additionally, the FT-IR spectra after adsorption showed the existences of stretching vibrations corresponding to the SO_3^- group of CR dye. Therefore, the electrostatic attraction between the SO_3^- groups of CR and the positive charge (OH_2^+) on the LDH sheets is predominantly responsible for the decontamination of the aqueous solution from azo dye. Besides, the presences of other weak interactions such as vander Waals, H-bonding, and surface complexation may also be prevalent.[41,43]

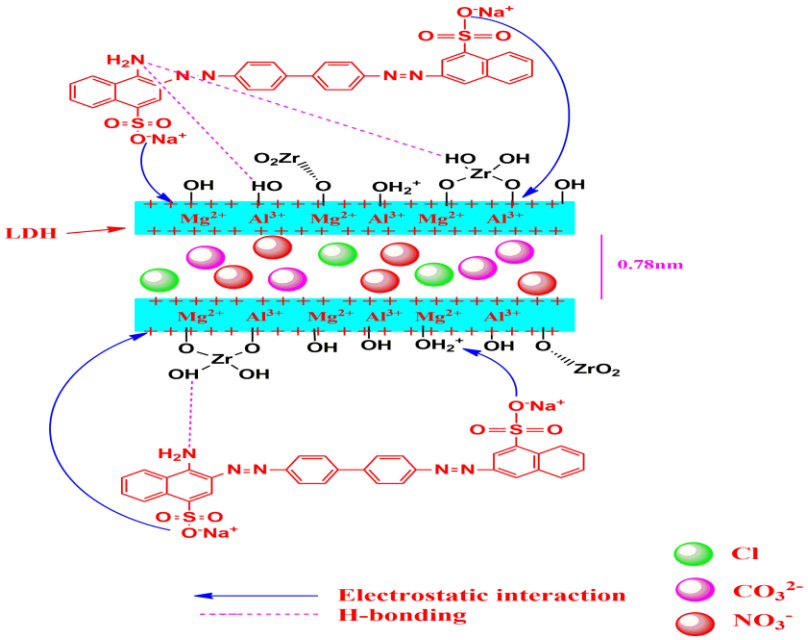

Fig II.17: Schematic representation of the plausible adsorption mechanism in CR adsorption on to ZrO_2/MgAl-LDH.

II.3.6 Reusability and Desorption studies:

Reusability performance of a material is an important aspect of evaluating the efficacy of an adsorbent for its industrial application. The reusability studies of ZrO_2/MgAl-LDH shown in **Fig II.18(a)** were investigated up to the fifth cycle under operating conditions fixed at an initial concentration of 50 mg/L, adsorbent dosages of 0.02 g, and contact time 6 hours. The initially adsorbed CR dye on the material surface was desorbed by dispersing in a 0.1M NaOH solution after each cycle. The alkaninity of the solution can decrease the strong electrostatic interaction between adsorbent and adsorbate, thereby leading to an easier desorption of CR dye. Subsequently, the regenerated adsorbent is dried and reuse up to the fifth cycle. From **Fig II.18(a)**, it is obvious that the adsorbent showed a reduction in its performance after each cycle. The maximum dye removal percentage in the first cycle showed up to 97.19 %, which slowly decreased to 59.04 % in the fifth cycle. The dye removal efficiency reduces to 38.15 % between the initial and last cycles. However, the decrease in adsorption capacity can be attributed to the loss of adsorption sites during the repeated regeneration process.[69]

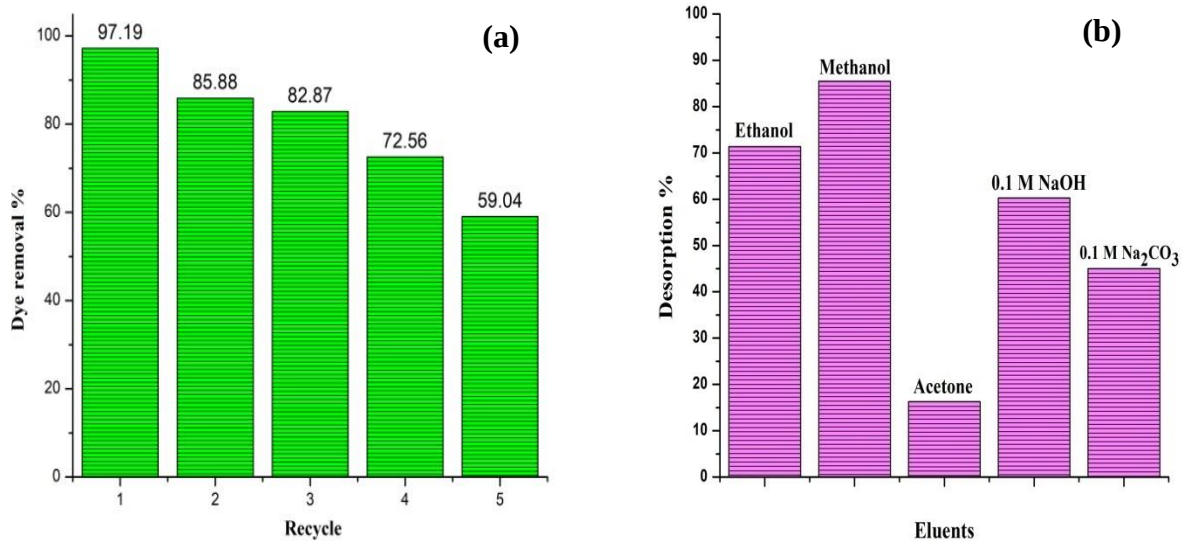

Fig II.18: (a) Reusability studies for the adsorption of CR dye by ZrO_2/MgAl-LDH (C_0 = 50 mg/L, adsorbent dosages = 0.02 g, volume = 20 mL, contact time = 6 hours). (b) Desorption percentage of CR dye from ZrO_2/MgAl-LDH at different eluents.

The graphical representation of the desorption studies conducted in various solvents is displayed in **Fig II.18(b)**. In an aqueous solution, the desorption activity of CR dye from the adsorbent ZrO_2/MgAl-LDH surface was not observed, thus indicating that adsorption process is completely opposite to the desorption process in an aqueous medium. However, the maximum desorption percentage of CR dye was obtained in a methanol solvent with 85.47 % desorption efficiency, which is comparatively higher than other desorbing eluents such as ethanol (71.37 %), acetone (16.28 %), 0.1M NaOH (60.27 %), and 0.1M Na_2CO_3 (45 %). The tendency to desorb CR dye in different solvents can be explained on the basis of their relative ability to weaken the strongly bound adsorbate-adsorbent interaction, especially electrostatic attraction and H-bonding. In solvents such as methanol and ethanol, the higher affinity towards the CR dye molecule may be attributed to the greater desorption percentage. In alkaline medium, desorption takes place due to hydrophobic interaction and greater anionic exchangeability between existing OH^- and CR ions over the positively charged adsorbent.[70, 71]

II.3.7 Comparison with reported adsorbents

With an emphasis on the maximum monolayer adsorption capacity shown by previously reported adsorbent for CR, the currently proposed adsorbent ZrO_2/MgAl-LDH displays a greater q_{max} value of 169.42 mg/g. In **Table II.5**, several adsorbents such as nanocrystalline hydroxyapatite, NiAl-LDH, MgAl-mixed metal oxide, and NiFeTi-LDH have relatively lower adsorption capacities than currently studied materials. Only a few of the materials, such as ZnAl-LDH and GO-NiFe-LDH, showed better performances than ZrO_2/MgAl-LDH. Besides, due to its facile synthetic procedure and comparatively remarkable higher sorption activity than most of the presented adsorbents, ZrO_2/MgAl-LDH can be regarded as the potential candidate for the efficient removal of CR dye from an aqueous solution.

Table II.5. The comparison of optimum experimental conditions for the removal of CR dye by several reported adsorbents.

Adsorbents	q_{max} (mg/g)	pH	Time (min)	Dosages (g)	Isotherm	References
NiFeTi-LDH	29.97	7	10	0.02	L	52
ZnAl-LDH	591.80	3	2-200	0.7	F	53
Cornuluca monacantha Stem	43.42	2	135	0.05	L	55
MgAl-mixed metal oxide	96.99	9	120	0.03	L	56
NiAl-LDH	120.5	6	30	0.01	L	63
Nanocrystalline Hydroxyapatite	139	5.5	20	2	F	72
MgAl-LDH/CF	271	3	4320	0.05	L	73
$Al(OH)_3$/CuMnAl-LDH	172	7	-	0.02	L	74
GO-NiFe-LDH	489	6-7	350	-	Liu	75
ZrO_2/MgAl-LDH	169.42	7	240	0.02	L	This work

Maximum monolayer adsorption capacity = q_{max} (mg/g), L= Langmuir, F=Freundlich, GO = Graphene Oxide

II.4 Conclusions

In this work, we have reported the synthesis of a novel tetravalent metal containing ZrO_2/MgAl-LDH and its potential adsorption performance towards CR dye. The as-synthesized ZrO_2/MgAl-LDH prepared by the urea hydrolysis method offers high crystallinity, porosity within the mesopore range, and an intermediate specific surface area of 71.55 m^2/g. The maximum removal of congo red was observed at the optimum pH of 4 for a contact time of 90

minutes. However, isotherm and kinetics analyses showed that the mechanism can be best described by the Redlich-Peterson, Langmuir, and pseudo second order kinetic models. In addition, the proposed adsorbent ZrO_2/MgAl-LDH revealed a higher uptake of CR (q_{max}=169.42 mg/g) compared to pristine MgAl-LDH previously reported. The thermodynamic parameter ΔG decreases with the increase in temperature from 301 to 333 K, indicating a spontaneous and endothermic process. The reusability tests up to the fifth cycle infers the superiority of the adsorbent materials. Moreover, this study has proposed a new approach to modify MgAl-LDH with tetravalent Zr^{4+} metal to enhance its sorption characteristics. The obtained results may encourage new emerging researchers and shed light on the need to further explore in designing of multivalent metal containing LDH for dye adsorption.

II.5 References

1. S. Benhaya, S. M′ rabbet, S, A.E. Harfi, *Inorg. Chem.Commun.*, 115, **2020**, 107891.
2. K, Abdellaoui, I. Pavlovic, C. Barriga, *ChemEngineering.*, 3, **2019**, 41.
3. R. Krishnamoorthy, A. Roy Choudhury, P. Arul Jose, K. Suganya, M. Senthikumar, J. Prabhakaran, N.O. Gopal, J. Choi, K. Kim, R. Anandham, T. Sa, *Appl. Sci.*, 11, **2021**, 379.
4. T. Shindhal, P. Rakholiya, S. Varjani, A. Pandey, H.H. Ngo, W. Guo, H.Y. Ng, M.J. Taherzadeh, *Bioengineered.*, 12, **2020**, 70-87.
5. W. Konicki, D. Sibera, U. Narkiewicz, *Sep Sci Technol.*, 53, **2018**, 1295-1306.
6. S.K. Sela, A.K.K. Nayab-Ul-Hossain, S.Z. Hussain, N. Hasan, *Clean. Eng. Technol.*, 1, **2020**, 100021.
7. B. Lellis, C.Z. Favaro-Polonio, J.A. Pamphile, J.C. Polonio, *Biotechnol. Res. Innov.*, 3, **2019**, 275-290.
8. J.N. Wekoye, W.C. Wanyonyi, P.T. Wangila, M.K. Tonui, *Environmental Chemistry and Ecotoxicology.*, 2, **2020**, 24-31.
9. S. Farhadi, F. Manteghi, R. Tondfekr, *Monatshe. Chem.*, 150, **2019**, 193-205.
10. B. Sherino, S.N.A. Halim, S. Shahabuddin, S. Mohamad, S. *Sep Sci Technol.*, 56, **2021**, 330-343.
11. N. Ali, A. Said, F. Ali, F. Raziq, Z. Ali, M. Bilal, L. Reinert, T. Begum, H.M.N. Iqbal, *Water Air Soil Pollut.*, 231, **2020**, 1-16.
12. M.R. Gadekar, M.M. Ahammed, *Appl. Sci.*, 10, **2020**, 1-8.
13. S. Natarajan, V. Anitha, G.P. Gajula, V. Thiagarajan, *ACS Omega.*, 5, **2020**, 3181-3193.
14. K. Ikehata, Y. Zhao, H.V. Kulkarni, Y. Li, S.A. Snyder, K.P. Ishida, M.A. Anderson, *Environ. Sci. Technol.*, 52, **2018**, 8588-8595.
15. Q. Wang, A. Tang, L. Zhong, X. Wen, P. Yan, J. Wang, *Powder Technol.*, 339, **2018**, 872-881.
16. R. Lafi, L. Gzara, R.H. Lajimi, A. Hafiane, *Chem. Eng. Process.: Process Intensif.*, 132, **2018**, 105-113.
17. N. Elhadiri, M. Benchanaa, R. Chikri, *J. Chem.*, 2020, **2020**, 2096834.
18. G. Moussavi, M. Mahmoudi, *J. Hazard. Mater.*, 168, **2019**, 806-812.
19. M.R. Abukhadra, A.S. Mohamed, *Silicon.*, 11, **2019**, 1635-1647.
20. X.S. Hu, R. Liang, G. Sun, *J. Mater. Chem. A.*, 6, **2018**, 17612-17624.
21. B. Mao, B. Sidhureddy, A.R. Thiruppathi, P.C. Wood, A. Chen, *New J. Chem.*, 44, **2020**, 4519-4528.
22. M. Munir, M.F. Nazar, M.N. Zafar, M. Zubair, M. Asfaq, A. Hosseini-Bandegharaei, S.U. Khan, A. Ahmad, *ACS Omega.*, 5, **2020**, 16711-16721.
23. M. Mohapi, J.S. Sefadi, M.J. Mochane, S.I. Magagula, K. Lebelo, *Crystals*, 10, **2020**, 957
24. M. Daud, A. Hai, F. Banat, M.B. Wazir, M. Habib, G. Bharath, M.A. Al-Harthi, *J. Mol. Liq.*, 288, **2019**, 110989.
25. R.K. Mahmoud, M. Taha, A. Zaher, R.M. Amin, *Sci. Rep.*, 11, 2021, 1-19.
26. S. Sonal, B.K. Mishra, *Chem. Eng. J.*, 424, **2021**, 130509.
27. R. Torres-Caban, C.A. Vega-Olivencia, N. Mina-Camilde, *Appl. Sci.*, 9, **2019**, 4531.
28. J.M. Jabar, Y.A. Odusote, K.A. Alabi, I.B. Ahmed, *Appl. Water Sci.*, 10, **2020**, 1-11.
29. I. Langmuir, *J. Am. Chem. Soc.*, 40, **1918**, 1361-1403.

30. S. Das, S.K. Dash, K.M. Parida, *ACS Omega.*, 3, **2018**, 2532-2545.
31. H.M.F. Freundlich, *J. Phys. Chem.*, 57, **1906**, 385-471.
32. M.I. Temkin, *Adv. Catal.*, 28, **1979**, 173-291.
33. O. Redlich, D.L. Peterson, *J. Phys. Chem.*, 63, **1959**, 1024-1024.
34. S. Sonal, P. Prakash, B.K. Mishra, G.C. Nayak, *RSC Adv.*, 10, **2020**, 13783-13798.
35. Y.S. Ho, G. McKay, *Process biochem.*, 34, **2020**, 451-465.
36. W.J. Weber, J.C. Morris, *J. Sanit. Eng. Div.*, 89, **1963**, 31-59.
37. M. Benjelloun, Y. Miyah, G.A. Evrendilek, F. Zerrouq, S. Lairini, *Arab. J. Chem.*, 14, **2021**, 103031.
38. S. Vahidhabanu, A.I. Adeogun, B.R. Babu, *ACS Omega.*, 4, **2019**, 2425-2436.
39. R. Benhiti, A.A. Ichou, A. Zaghloul, R. Aziam, G. Carja, M. Zerbet, F. Sinan, M. Chiban, *Environ. Sci. Pollut. Res.*, 27, **2020**, 45767-45774.
40. A. Nuryadin, T. Imai, *Glob. J. Environ. Sci.*, 7, **2021**, 485-502.
41. J. Poonoosamy, F. Brandt, M. Stekiel, P. Kegler, M. Klinkenberg, B. Winkler, V. Vinograd, *Appl. Clay Sci.*, 151, **2018**, 54-65.
42. A.K. Avila-Martinez, J.H. Roque-Ruiz, J. Torres-Perez, N.A. Medellin-Castillo, S.Y. Reyes-Lopez, *Eniviron. Technol. Innov.*, 18, **2020**, 100760.
43. R. Shabbir, A. Gu, J. Chen, M.M. Khan, P. Wang, Y. Jiao, Z. Zhang, Y. Liu, Y. Yang, *Int J Environ Anal Chem.*, **2020**, 1-18.
44. O.S. Travkina, M.R. Agliullin, R.Z. Kuvatova, I.N. Pavlova, N. Narender, B.I. Kutepov, *J. Porous Mater.*, 26, **2018**, 995-1004.
45. B. Priyadarshini, T. Patra, T.R. Sahoo, *J Magnes. Alloys.*, 9, **2021**, 478-488.
46. V.R. Magri, A. Duarte, G.F. Perotti, V.R.L. Constantino, *Chemengineering*, 3, **2019**, 55.
47. S. Naseem, B. Gevers, R. Boldt, F.J.W.J. Labuschagne, A. Leuteritz, *RSC Adv.*, 9, **2019**, 3030-3040.
48. C. Hobbs, S. Jaskaniec, E.K. McCarthy, C. Downing, K. Opelt, K. Guth, A. Shmeliov, M.C.D. Mourad, K. Mandel, V. Nicolosi, *NPJ 2D Mater. Appl.*, 2, **2018**, 1-10.
49. J. Zhu, Z. Zhu, H. Zhang, H. Lu, Y. Qiu, *RSC Adv.*, 9, **2019**, 2284-2291.
50. P. Lackner, Z. Zou, S. Mayr, U. Diebold, M. Schmid, *Phys. Chem. Chem. Phys.*, 21, **2019**, 17613-17620.
51. Z. Azdad, L. Marot, L. Moser, R. Steiner, E. Meyer, E. *Sci. Rep.*, 8, **2018**, 1-6.
52. G. Rathee, A. Awasthi, D. Sood, R. Tomar, V. Tomar, R. Chandra, *Sci. Rep.*, 9, **2019**, 1-14.
53. A.E. Khanchaoui, M. Sajieddine, M. Mansori, A. Essoumhi, *Int J Environ Anal Chem.*, 102, **2020**, 1-19.
54. S. Popa, M.E. Radulescu-Grad, A. Perdivara, G. Mosoarca, *Sci. Rep.*, 11, **2021**, 1-9.
55. A. Sharma, Z.M. Siddiqui, S. Dhar, P. Mehta, D. Pathania, *Sep. Sci. Technol.*, 54, **2019**, 916-929.
56. Y. Lv, L. Gao, S. Feng, S.; Wang, Y. Qiao, Q. Li, *Sep. Sci. Technol.*, 54, **2019**, 2625-2637.
57. N.I. Blaisi, M. Zubair, Ihsanullah, S. Ali, T.S. Kazeem, M.S. Manzar, W. Al-Kutti, M.A. Al Harthi, *Environ. Sci. Pollut. Res.*, 25, **2018**, 34319-34331.
58. N.K. Gupta, M. Saifuddin, S. Kim, K.S. Kim, *J. Mol. Liq.*, 297, **2020**, 111935.
59. Y. Chen, C. Jing, X. Zhang, D. Jiang, X. Liu, B. Dong, L. Feng, Li.; S. Li, Y. Zhang, *J. Colloid Interface Sci.*, 548, **2019**, 100-109.
60. G.Y. Abo El-Reesh, A.A. Farghali, M. Taha, R.K. Mahmoud, *Sci. Rep.*, 10, **2020**, 1-20.

61. S. Dutta, B. Gupta, S.K. Srivastava, A.K. Gupta, *Mater. Adv.*, 2, **2021**, 4497-4531.
62. R. Gopinathan, A. Bhowal, C. Garlapati, *J. Chem. Eng. Data*, 64, **2019**, 2320-2328.
63. D. Bharali, R.C. Deka, *J. Environ. Chem. Eng.*, 5, **2017**, 2056-2067.
64. L. Jiang, Y. Liu, S. Liu, X. Hu, G. Zeng, X. Hu, S. Liu, S. Liu, B. Huang, M. Li, *Chem. Eng. J.*, 308, **2017**, 597-605.
65. P.K. Singh, S. Banerjee, A.L. Srivastava, Y.C. Sharma, *RSC Adv.*, 5, **2015**, 35365-35376.
66. X. Zheng, X. Li, J. Li, L. Wang, W. Jin, J. Liu, Y. Pei, K. Tang, *Int. J. Biol. Macromol.*, 107, **2018**, 283-289.
67. V.O. Shikuku, R. Zanella, C.O. Kowenje, F.F. Donato, N.M.G. Bandeira, O.D. Prestes, *Appl. Water Sci.*, 8, **2018**, 1-12.
68. Y. Li, H.Y. Bi, Y.S. Jin, X.Q. Shi, *RSC Adv.*, 4, **2014**, 58307-58314.
69. D.N. Ahmed, L.A. Naji, A.A.H. Faisal, N. Al-Ansari, M. Naushad, *Sci. Rep.*, 10, **2020**, 1-12.
70. E. Rapo, S. Tonk, *Molecules.*, 26, **2021**, 5419.
71. D. Brahma, H. Saikia, *Chem. Thermodyn. Therm. Anal*., 7, **2022**, 100067.
72. H. Bensalah, S.A. Younssi, M. Ouammou, A. Gurlo, M.F. Bekheet, *J. Environ. Chem. Eng.*, 8, **2020**, 103807.
73. Q. Sun, B. Chen, *Ind. Eng. Chem. Res.*, 59, **2020**, 16838-16850.
74. J.O. Eniola, R. Kumar, A.A. Al-Rashdi, M.O. Ansari, M.A. Barakat, *ACS Omega.*, 4, **2019**, 18268-18278.
75. Y. Zheng, B. Cheng, W. You, J. Yu, W. Ho, *J. Hazard. Mater*., 369, **2019**, ,214-225.